Optimization of a Horizontal Axis Tidal (HAT) turbine for powering a Reverse Osmosis (RO) desalination system using Computational Fluid Dynamics (CFD) and Taguchi method

Mohammad Hassan Khanjanpour, Akbar A. Javadi*

Department of Engineering, University of Exeter, Exeter, EX4 4QF, UK.

*Corresponding author

*Akbar A. Javadi

Tel: +44 1392 723640,

Email: A.A.Javadi@exeter.ac.uk

Abstract

Horizontal Axis Tidal (HAT) turbines can be used to power RO (reverse osmosis) desalination systems. The greatest weakness of these turbines is the high price of design, development, and manufacturing. Traditionally, optimization of turbine geometry is achieved by running several numerical models of the turbine which can become time consuming and expensive. The Taguchi-CFD (Computational Fluid Dynamics) approach has recently been introduced as an inexpensive and rapid tool for optimizing industrial devices. This technique can be used as a straightforward solution for optimization of geometry of HAT turbines. In this work, a conceptual design of a tidal power reverse osmosis (TPRO) desalination unit was proposed. Subsequently, the geometry of the HAT turbine, which can power the whole desalination system, was optimized with combination of only 16 CFD simulations using the Taguchi method. The effects of blade size, number of blades, hub radius, and hub shape were studied and optimized. The Taguchi results revealed that the most important parameters influencing the power output of HAT turbine are the number of blades, size of blade, hub radius, and hub shape respectively. Moreover, the results of the superposition model showed that the minimum signal-to-noise ratio (SNR) is 21% less than the amount achieved in the Taguchi approach. The power coefficient (C_p) of the optimized HAT turbine was 0.44 according to the results of CFD simulations, which was 10% higher than that of the baseline model (0.40) at tip speed ratio (TSR) of 5. The weight of the optimized model was less than the baseline model by 17%. The results of this study provide a comprehensive guidance for horizontal turbine optimization process.

Keywords: HAT Turbine, Desalination, Taguchi method, ANOVA, signal-to-noise ratio, Computational fluid dynamics.

Nomenclature (alphabetical order)

ANOVA	Analysis of variance	RO	Reverse osmosis
A_t	Area of the blades (m^2)	R	Turbine radius (m)
C_p	Power coefficient	S	Area of a blade (m^2)
C_m	Torque coefficient	SNR	Signal-to-noise ratio
ED	Electrodialysis	SST	Shear Stress Transport
ERD	Energy recovery device	T	Torque (N.m)
G	Calculated response	TPRO	Tidal power reverse osmosis
HAT	Horizontal Axis Tidal	TSR	Tip speed ratio
L	Distance from center of hub (m)	T_c	computed response
MVC	Mechanical vapor compression	T_q	Target quality
n	number of experiments	U_∞	Water velocity (m/s)
n_b	Number of blades	VAT	Vertical Axis Tidal
OA	Orthogonal array	X	Quadratic loss factor
P	Power output (W)	α	Solidity ratio
P_n	Nominal output power (W)	β	Impact of each factor
PISO	Pressure Implicit Splitting of Operator	ρ	Water density (kg/m^3)
PV	Photovoltaic	ψ	Mean of total mean SNRs
Q	Indicator blade	ψ^t	Predicted SNR
QLF	Quadratic loss function	ω	Angular velocity (rad/s)

1. Introduction

Water crisis is among the serious challenges that threatens human society's sustainable development [1, 2]. According to a new report by WHO and UNICEF, by 2025, 1.8 billion people will be living in countries or regions with absolute water scarcity [3, 4]. Even countries that are currently rich in water resources, will face water shortage in future. Figure 1 shows the water availability indicators due to climate change and population growth in the UK for 2050s [5]. The indicator of water availability, which varies from -1 to 1, identifies the ratio of excess water consumption over water supply of the most challenging months during the prediction period. It can be seen from Figure 1 that, even a country like UK will experience water scarcity in coming decades. Fortunately, since about 71% of the Earth's surface is covered with water [6], one of the solutions for world's water crisis can be seawater desalination. However, seawater desalination requires a significant amount of energy [7-10].

Most of the existing desalination systems are powered by energy from burning of fossil fuels [11, 12]. Renewable energy, in many cases, can be utilized to power desalination devices [13, 14]. Tidal energy, utilizing ocean tidal currents, provides a reliable renewable resource with the advantage of being highly predictable many years into the future and significantly greater in its energy density compared to wind and solar energies, albeit intermittent on a daily or twice-daily time-scale [15]. Ocean powered seawater desalination has become a new approach for desalination due to the above-mentioned advantages [16-22]. However, the development of ocean powered seawater desalination technologies is at its infancy and more investigation is needed before fully operational systems are deployed and implemented.

Zhao and Liu [23] carried out a theoretical study on a tidal-powered solar distillation system. In their innovative design, instead of running pumps with electricity, tidal energy was used to produce energy for vacuum extraction as well as water intake. They performed hydrodynamic and thermal analysis for the water intake and drainage system powered by tidal energy. Their proposed system can only work efficiently in locations with a tidal level greater than 2 m, however, using storage tank can stabilize energy requirement when tidal energy is used for powering water pump. A wave-powered RO desalination system was developed by Sharmila et al. [24] in India. Since waves are transient and irregular source of energy throughout the year, it is essential to predict the behavior of the system at various wave energy rates. Thus, they theoretically simulated the wave energy profile and based on the obtained profile, they designed and developed a wave converter that was suitable for the desalination system. Unlike wave energy which is influenced by speed of the wind, the strength of tidal energy is influenced by the location and shape of the Earth which makes tidal energy quite predictable [25]. Ling et al. [26] carried out an economic analysis of a TPRO desalination system where the productivity of the desalination system and cost of freshwater were compared with other methods. It was concluded that the TPRO desalination system could save water costs between 30- 40% compared to the traditional RO system.

Tidal turbines, including the Vertical Axis Tidal (VAT) turbine and Horizontal Axis Tidal (HAT) turbine, can be used to power desalination systems. A HAT turbine contains a radial axis rotor which is parallel to the water stream. With its drag or lift style blades, which are usually perpendicular to the rotational axis, it can convert the kinetic energy of water to mechanical energy [27]. In VAT turbines, the radial axis rotor is perpendicular to the water stream and, similar to HAT turbines, their blades can be either drag or lift style [28]. Since the greatest weakness of tidal

turbines is the high cost of development and fabrication, using an inexpensive Taguchi method can be helpful for turbine developers to reduce design costs.

The Taguchi method, also known as the Robust Design method, is one of the powerful optimization techniques in product design [29]. The fundamental principle of the Taguchi method is to increase the efficiency of a product by reducing the number of tests required without eliminating any parameters [30]. The Taguchi approach provides Orthogonal Arrays (OA) for the execution of minimal tests to include a wide variety of variables for improved decision-making. It also uses the signal-to-noise ratio (SNR) to measure the divergence of the output, from the target value. The SNR is a criterion for quality assessment, and the OA is to provide minimal design parameters simultaneously [31]. The target quality of performance is a key factor in the Taguchi approach and must be indicated for each optimization procedure. It is possible to integrate the Taguchi method with Computational Fluid Dynamic (CFD) models (the same way as other optimization models have been combined with CFD [e.g., 32, 33]) to predict optimized factors.

Wang et al. [34] improved the performance of a vertical wind turbine by using the CFD-Taguchi method. They characterized design parameters such as wave amplitude, wavelength, and twist angle while the objective function was the power coefficient (C_p). For the Taguchi method they used a standard L9 (3^4) OA. By accomplishing only nine CFD tests, they improved the output of the vertical axis wind (VAW) turbine by 18%. Recently, Khanjanpour and Javadi [35], optimized the efficiency of a VAT turbine combining a mixed-level L_{18} (6^1*3^3) Taguchi with 18 CFD simulations. They studied the effects of ratio of chord/radius, maximum camber, camber position, and twist angle on the performance of the VAT turbine. Their findings showed that, compared to the initial design, the power output for the optimized VAT turbine was enhanced by 24%.

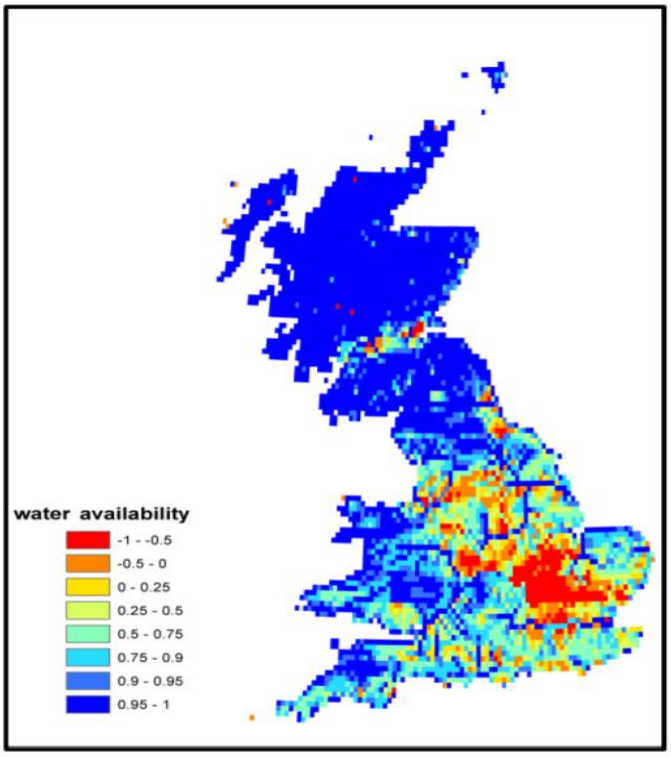

Figure 1. Water availability indicator for 2050s in the UK [5].

The main objective of the current work is to design and optimize the geometry of a HAT turbine for powering a desalination system. Review of the previous research shows that the influence of combinations of size of blades, number of blades, hub radius, and hub shape on the power output of HAT turbines has not been investigated. The goal of optimization of these factors is to find a lighter, cheaper and smaller turbine which can be used in shallow water. For this purpose, the Taguchi method is used to optimize the turbine in order to identify a cost-effective geometry for use in a RO desalination system. By using the Taguchi method and only 16 CFD simulations, the effects of size of blades, number of blades, hub radius, and hub shape on power output of HAT turbine are studied. Finally, a new range of optimized variables is defined and evaluated. In addition, the dynamics of the fluid flow across the optimized and initial turbines is studied and compared.

In what follows, the design of the desalination system is presented in Section 2. In Section 3, the details of a preliminary design of the baseline HAT turbine are given. Section 4 presents CFD simulation of the baseline turbine and validation of the model. In Section 5 the Taguchi method and the superposition model are used to find the optimum parameters of the turbine. In Section 6, a comprehensive CFD simulation of the baseline and the optimized cases is presented. Finally, Section 7 presents the conclusions and some recommendations for future work.

2. Design of the desalination system

2.1. Location of the desalination system

One of the prerequisites of development of a tidal seawater desalination system is to find coastal areas with high-speed current, particularly in regions with low salinity, as salinity can affect the energy consumption of RO unit [36]. Figure 2 illustrates the current speed and seawater surface salinity around the UK. From this figure, it can be seen that there are numerous locations, which are suitable for tidal-powered desalination system, especially in the straits and in narrow places that have an appropriate space for harnessing tidal energy. The coastline of South East England is suitable for installation of a TPRO desalination system; not only it has low salinity and high current speed, but also in future it will have a higher demand for water (see Figure 2). Accordingly, for the rest of this research, the mean tidal current velocity and salinity of water are assumed as 1 m/s and 30 ppt respectively.

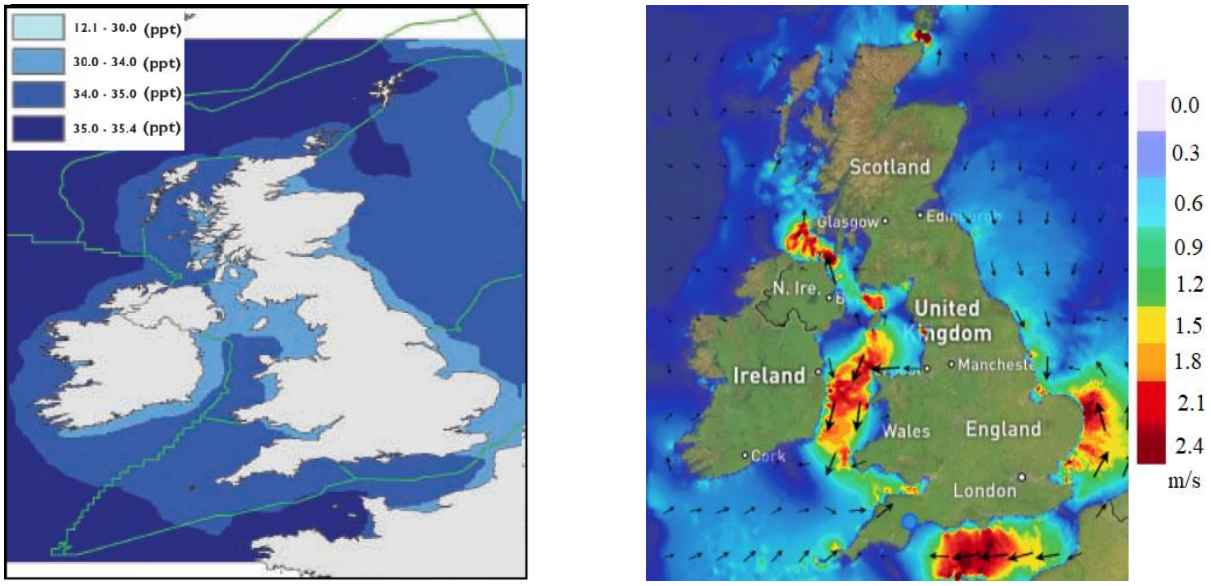

(a) (b)

Figure 2. (a) The current speed [37] and (b) seawater surface salinity around UK [38].

2.2. RO unit

A wide range of desalination technologies are available for producing fresh water from seawater. Although some desalination devices are available commercially, most of them are in the early stage of research and development. The selection of appropriate technology is affected by the nature of the water source, the amount of collected water, and most importantly, the total energy consumption [39]. The three most common systems that can be combined with sea power are reverse osmosis (RO), electrodialysis (ED), and mechanical vapor compression (MVC) [40]. The best desalination method which can be combined with tidal energy is Reverse Osmosis [41, 42]. Figure 3 shows a schematic of a membrane of a reverse osmosis unit. RO is a process where pressurized seawater flows through a semipermeable membrane, separating freshwater from saline water. The chemical potential of the solute, depending on temperature, salinity and pressure, is to be equal on both sides of the membrane. By adding an external pressure to one side of the

membrane, clean water will flow to the other side to restore the chemical potential. The products of the RO process are freshwater and the residue (concentrate or brine) of high salinity. The RO method has unique advantages such as adjustable size and low price (almost 25% less than thermal options), therefore, in this study RO is selected for the desalination system [43]. Recently, there has been significant research on the use of RO system for sustainable water production [44-47]. The characteristics of the membrane identify its capacity to enable water to be preferentially transported over the solute. To ensure that water passes through the membrane, the pressure difference between the feed part and the membrane permeate side should be considerably higher than the osmotic pressure. This working pressure of RO must be about 3-5 bar according to existing studies [48], however, several qualified RO industries are designing innovative products which could be utilized with much less pressure [49].

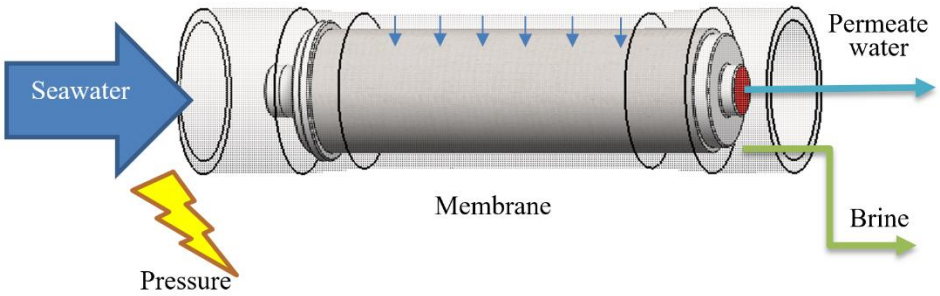

Figure 3. Schematic of a membrane of RO unit [50].

2.3 Conceptual design of the TPRO desalination system

A schematic of the conceptual design of TPRO desalination system using HAT turbine is illustrated in Figure 4, adapted from reference [51]. The main components of the design and their functions are as follows:

193 (1) Tidal turbine: powers the high-pressure pump and fills the water storage tank, (2) Water storage
194 tank: stabilizes the driving energy, (3) High-pressure pump: moves and pressurizes water from the
195 sea to the RO unit and water tank, (4) RO unit: desalinates saline water, (5) Booster pump: pumps
196 output water from energy recovery device (ERD) to the RO unit, (6) ERD: recovers the energy of
197 water output of RO unit, and (7) PV (Photovoltaic) panel and battery: provide the required
198 electricity for the booster pump.

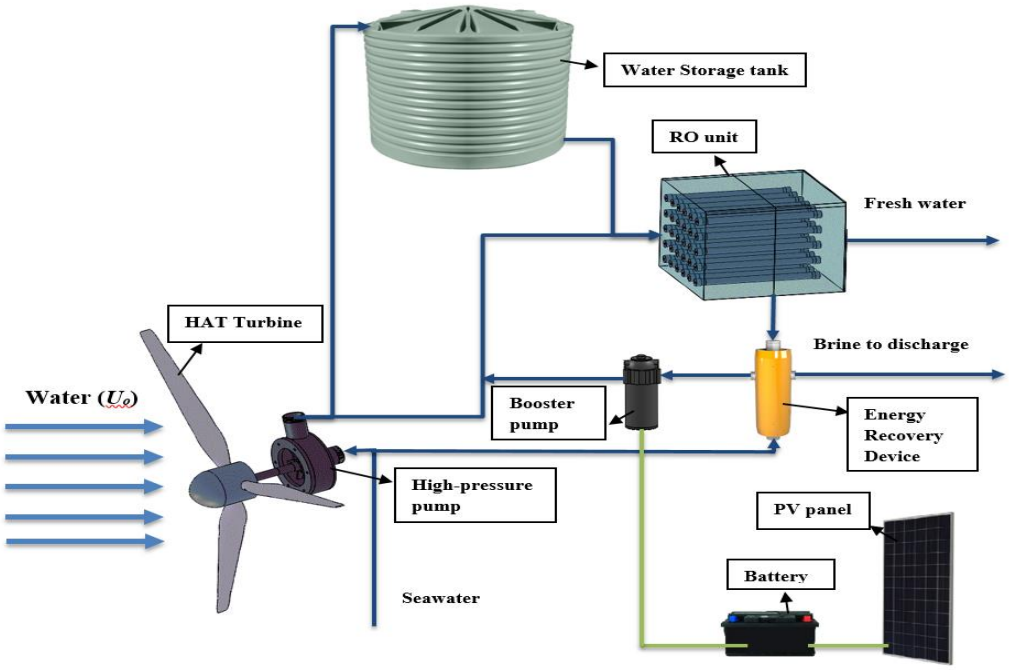

Figure 4. Schematic of the RO desalination system using a HAT turbine.

199

200 The HAT tidal turbine extracts energy from the sea and runs the high-pressure water pump in order
201 to provide the hydraulic pressure needed for the RO unit. In the proposed conceptual design, there
202 is no need to convert kinetic energy to electricity in a generator, and then electricity to kinetic
203 energy in an electric motor and finally use the kinetic energy to pressurize water in a pump. The
204 kinetic energy is used directly to pressurize the water in the RO system. Moreover, the electricity

harnessed from tidal power is usually wasted due to limited consumption during off-peak hours. With proposed conceptual design, the turbine uses tidal energy to run a water pump and when the system has adequate pressurized water, the energy of the movement can be stored in the water storage tank to stabilize the driving energy.

Most of the components of the proposed system are available in the market and various companies offer these goods on a large scale. However, tidal turbine which is the most expensive and complex part is not supplied as a whole package. Therefore, in this study the tidal turbine is selected to be optimized to identify the smallest and cheapest geometry, which can provide the required power for the desalination system.

2.4. Energy required for desalination

In this section, the pressure required for desalinating 1 m^3/h is determined. Some assumptions are necessary to estimate this pressure. The proposed conceptual desalination system has three major energy requirements: (1) energy for the RO unit, which has the highest energy consumption in the desalination systems [52-56], (2) energy for pumping of the seawater from the nearshore to the system, and (3) electricity consumption in the booster pump, which is used after ERD to pump water to the RO unit.

Energy consumption for modern RO desalination systems is between 2000-4000 Wh/m^3 [17, 57, 58]. By using a more efficient ERD, the energy consumption inside the RO unit can be assumed as 2400 Wh/m3 for seawater with salinity of 30 ppt [59]. The energy usage for transferring seawater to RO unit and the storage tank in a standard desalination system is about 200 Wh/m^3 [60]. According to Khanjanpour and Javadi [61], changes in roughness of the blades due to sticky sea animals and corrosion can decrease the performance of tidal turbines by about 20%. In

addition, CFD simulations considering rigid body geometries, ignores the turbine blade hydroelastic behavior. Accordingly, vibration and deformation can adversely influence the performance of the turbines. Therefore, an additional 10% is added to the energy consumption due to this shortcoming of CFD simulations in order to determine the required power [62]. Finally, the total energy that should be provided by the turbine is estimated as 3440 Wh/m^3. It should be noted that this is a safe value for the worst-case scenario, and obviously, if the amount of roughness and deformation can be controlled by using better materials, this value could be less than 3440 Wh/m^3. A Photovoltaic (PV) panel and a battery storage are proposed to power booster pump.

3. Preliminary design of the baseline HAT turbine

As mention above, the HAT turbine is designed to provide 3440 W to power RO desalination system for producing 1 m^3/h freshwater. The well-known equations of horizontal turbines are used to estimate this power. The real power output is described as the power coefficient (C_p) multiplied by nominal power output (P_n) (Eq. 1) [63]. The nominal power output can be calculated from the turbine geometry as well as the flow characteristics based on the particular application [64]. For initial design of the baseline HAT turbine, some basic assumptions are considered based on the literature. According to the experimental work by Bahaj et al. [65], the maximum value of C_p of 0.3 is considered for the tidal turbine, as a safe estimate, to determine the baseline turbine geometry.

$$P = P_n C_n \tag{1}$$

where P is power output, P_n is nominal power, and C_p is power coefficient.

The nominal power can be calculated as [66]:

$$P_n = \frac{\rho 2\pi R^2 U_\infty^3}{2} \quad (2)$$

where ρ is the water density, U_∞ is the velocity of water, and R is the turbine radius (distance between the center of hub to the blade tip).

With the above-mentioned values for the power output and maximum power coefficient, and considering the inlet water velocity as 1 m/s, the initial parameters of the baseline HAT turbine are determined as summarized in Table 1.

Table 1. Initial parameters of HAT Turbine

Total length of blade	Root length	Type of hydrofoil	Hub radius	Number of blades
1.2 m	0.24 m	NACA 0018	0.2 m	3

The related literature [67-69] has been used to design an efficient blade in order to achieve highest hydrodynamic performance. Accordingly, a model blade of 1.2 m is designed for the baseline turbine with SOLIDWORKS 2017, using the methodology outlined in [70]. The blade is designed by using NACA 0018 profile with different distances from the hub circle and different twist angles. According to previous publications, the distance from the hub circle to the root airfoil chord is selected as 0.24 m, which is 20 % of the total blade length, and the twist angles for root and tip sections are varied from 18^o to 3^o. Details of the NACA 0018 stations and designed blade are presented in Table 2 and Figure 5. Using the values in Table 1 and the designed blade, the baseline HAT turbine is designed in the SOLIDWORKS software, the details of which are shown in Figure

6.

Table 2. Blade parameter

Section	Twist angle (°)	L (m)
Root	18	0.24
Station 1	14	0.36
Station 2	12	0.48
Station 3	10	0.60
Station 4	8	0.72
Station 5	7	0.84
Station 6	5	1.01
Station 7	4	1.12
Tip	3	1.20

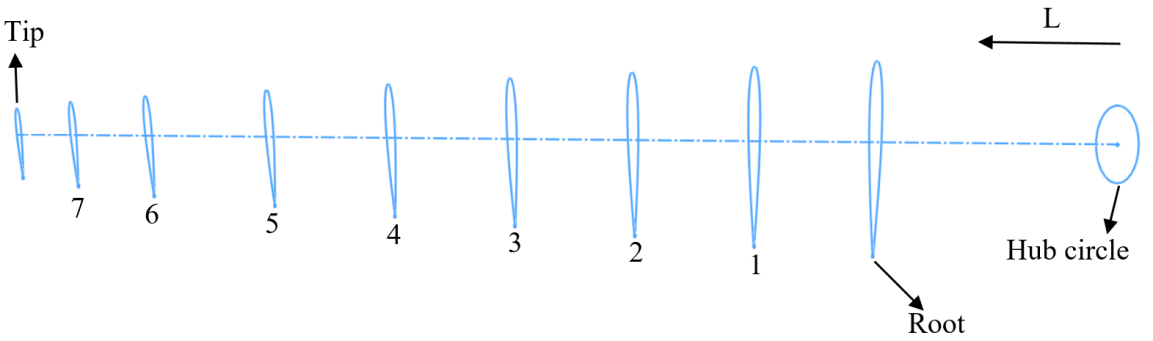

(a)

(b)

Figure 5. (a) Definition of the NACA 0018 stations and (b) designed blade.

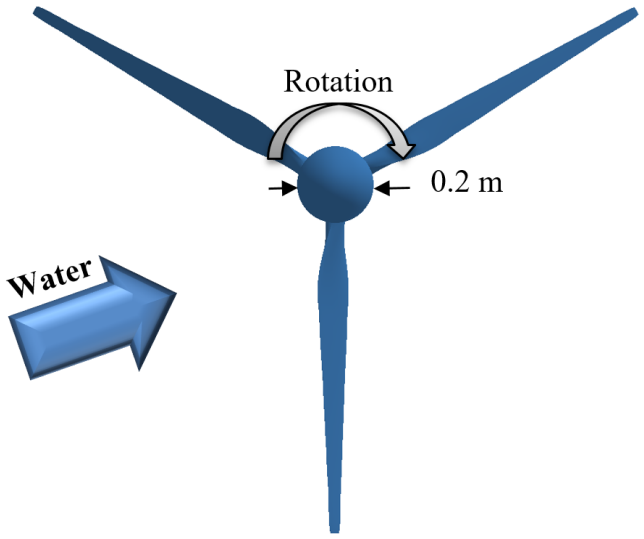

Figure 6. 3D design of the baseline HAT turbine.

4. CFD simulation and validation of the baseline turbine

Figure 7 shows the details of the computational domain, mesh intensity around the turbine, and boundary conditions. An unstructured mesh is built around the turbine and a structured one over the entire computational domain by using the ICEM 2019 software. A three-dimensional transient model is built for CFD simulations of the HAT turbine using ANSYS Fluent. In addition, a sliding mesh method is used for simulating the movement of the fluid around the turbine. For the CFD simulations in ANSYS Fluent, the Shear Stress Transport (SST) k-ω turbulence method and the Pressure Implicit with Splitting of Operator (PISO) algorithm are implemented [71]. A computer with 28-core Intel CPU E5-2680 v4 Processors, 256GB RAM is used to run the CFD simulation.

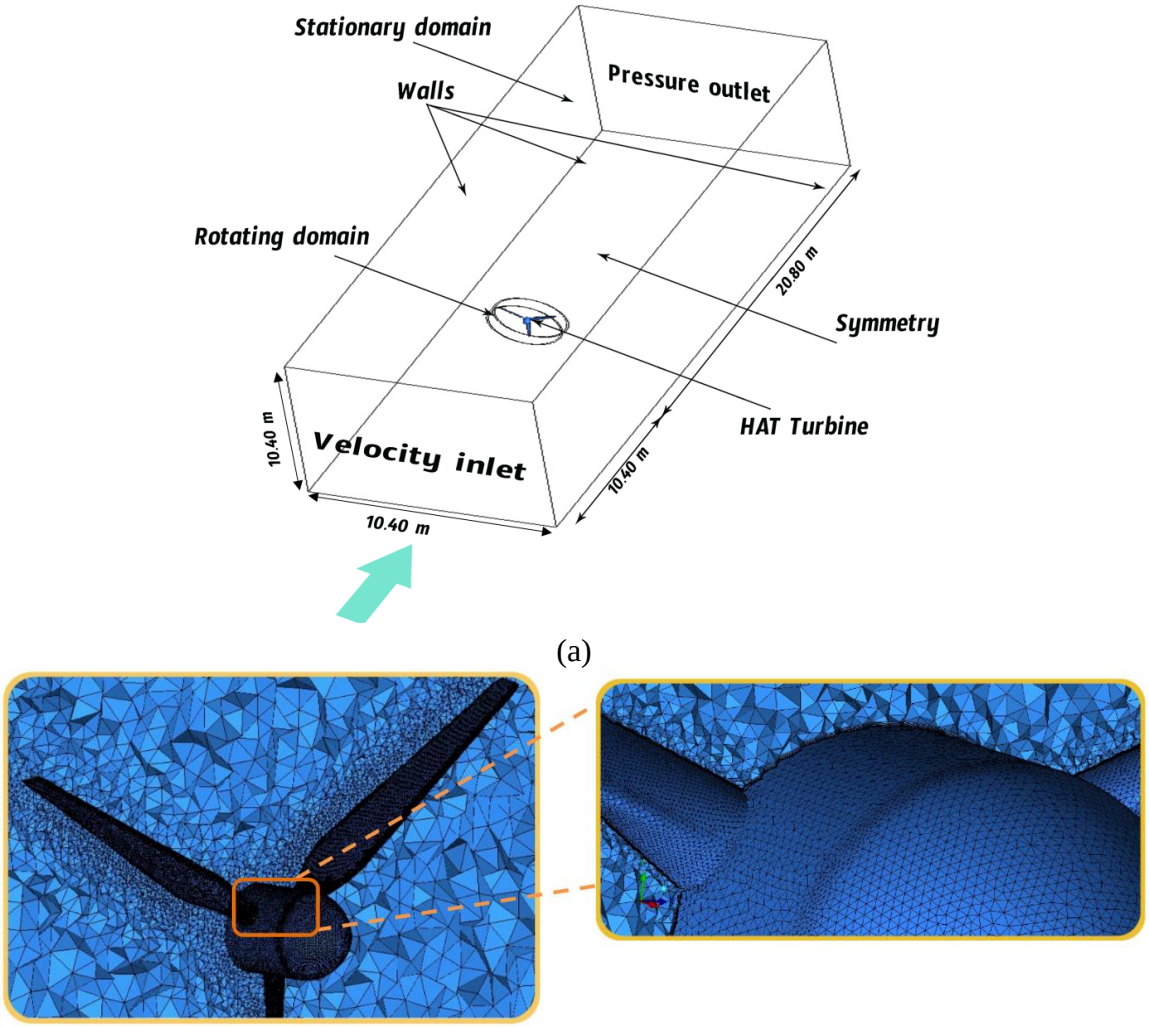

(a)

(b)

Figure 7. (a) Computational domain and boundary conditions and (b) mesh intensity over the turbine.

281

282 A mesh sensitivity analysis is carried on by generating eight different meshes (from 598,771 cells
283 to 6,981,342) for the baseline design using ICEM CFD software. Using Eq. 3 and the CFD
284 simulation results, the torque coefficient (C_m) is determined for each case with varying numbers
285 of cells and the results are presented in Figure 8. The study revealed that beyond 2,395,084 cells,
286 the standard deviation of the torque coefficient is around 1.0%. As the computational time of the
287 numerical analysis increases dramatically with the number of cells, 2,395,084 is selected for the

rest of the CFD simulations. The simulation time with 2,395,084 cells is 46 hours by using the above-mentioned computer.

$$C_m = \frac{T}{0.5\rho A_t U_\infty^2} \quad (3)$$

where C_m is the torque coefficient, T is the torque, and A_t is the area of the blades.

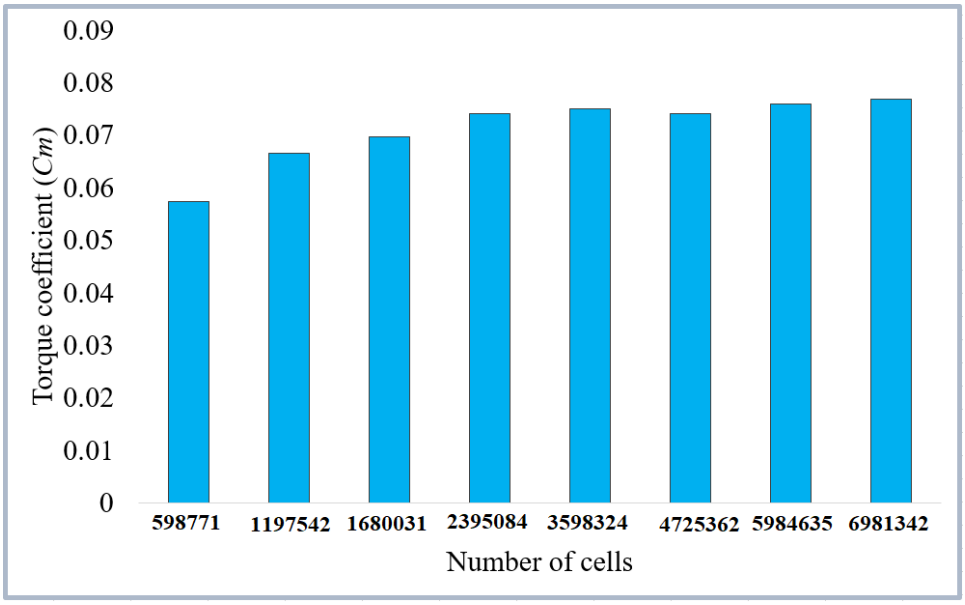

Figure 8. Torque coefficient (C_m) vs. number of cells for grid sensitivity analysis

One of the common methods to validate CFD model for turbines simulation is assessing C_p against TSR. The power coefficient (C_p) of a HAT turbine can be determined as follows [69]:

$$C_p = (TSR)C_m \quad (4)$$

Using Eqs. 3 & 4 and the CFD results, the values of power coefficient at various TSRs are determined and the results are shown in Figure 9. Also, the variations of C_p with TSR for an

experimental work reported by Bahaj et al. [65] and a CFD study by Kulkarni [70] are provided in Figure 9 to validate the current CFD model. According to Figure 9, the results of the current CFD model are in good agreement with the experimental and CFD results of [64] and [69], both in terms of values and patterns.

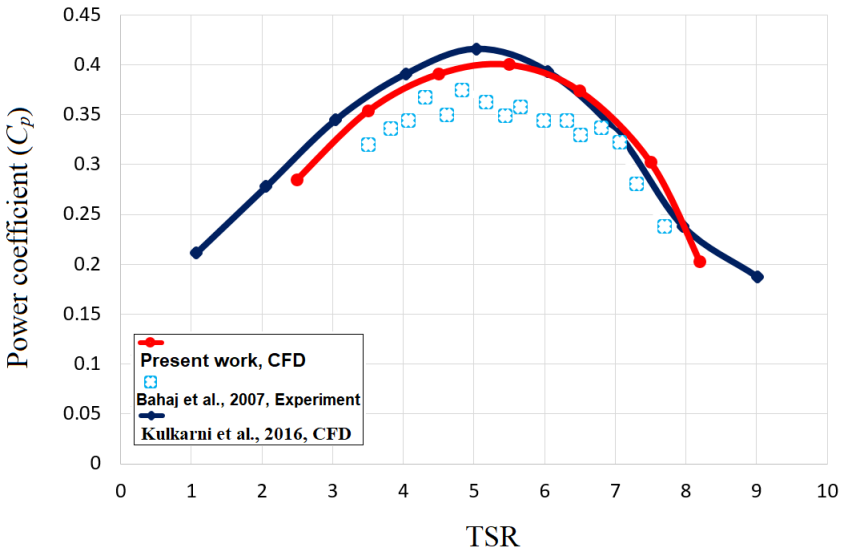

Figure 9. Variation of C_p with Tip speed ratio (TSR), used for model validation.

5. Taguchi method

The Taguchi method offers an affordable and effective way for minimal series of experiments to find optimal parameters of a system [72]. It uses a signal-to-noise ratio (SNR) to quantify the difference in responses. The Taguchi method is commonly employed for a wide range of optimization problems. The identification of the optimum factors and levels can be divided into 7 stages [73].

Stage 1: Determination of the objective function

To determine the objective function, a quadratic loss function (QLF) (Eq. 5) is defined to calculate the divergence of a variable from its target quality [74].

$$QLF = X(T_c - T_q)^2 \quad (5)$$

where X is the quadratic loss factor, T_q is the target quality, and T_c is the computed response.

The QLF can estimate quality loss in a meaningful way [34, 35] . In this study, power output is considered as the quality target in the objective function. For calculating SNR, there are three approaches in the Taguchi method: Larger is the better, Nominal is the Best, and Smaller is the better [75]. Because the aim of this analysis is to minimize the Quality Loss Function, in this research the Smaller the better SNR formula is used as follows [76]:

$$\text{Smaller is the better: } SNR = -10\, log \frac{1}{n} \sum_{i=1}^{n} (G_i)^2 \quad (6)$$

where n: the number of experiments; G: the calculated response.

To quantify a parameter's deviation from its target value, the QLF can normally be modified to an SNR as [77]:

$$SNR = 10 \log(T_c - T_q)^2 \quad (7)$$

According to the results presented in section 2.4, by replacing power output and target quality, the objective function can be redefined as:

$$SNR = 10 \log(P - 3440)^2 \quad (8)$$

Stage 2: Definition of factors and levels

The Taguchi method is employed to analyze the impacts of different factors (control factors), in order to optimize the main parameters of a system. The objective of this method is to estimate the optimal combination of control factors and their levels. A horizontal turbine consists of two main parts: the hub and the blades. The solidity ratio, which is the most important factor affecting turbine performance [78, 79], is described as the ratio of the total turbine blade area over the swept area [80]. The solidity ratio for HAT turbine can be calculated as [81, 82]:

$$\alpha = \frac{n_b S}{\pi r^2} \tag{9}$$

where α is the solidity ratio, n_b is the number of blades, and S is the area of a blade.

According to Eq. 9, the solidity ratio varies greatly with the blade size and the number of blades. Thus, optimization of this ratio is accomplished by changing these two factors. On the other hand, the type of hub can be changed based on the hub radius and shape of the hub.

In this work, four factors are considered to be optimized including size of blade (A), number of blades (B), hub radius (C), and hub shape (D). In addition, for each factor four levels are considered.

Due to the submergence of the tidal turbines in water, their working conditions vary from the wind turbines; HAT turbines face higher torque and pressure than horizontal axis wind (HAW) turbines. Therefore, tidal turbines must have smaller blades to avoid vibration and deformation which unfavorably affect the turbine efficiency [83-85]. Accordingly, four sizes of blade including 0.7b, 0.8b, 0.9b, and 1.0b (b is the size of blade according to Tables 1 and 2) for HAT turbine are chosen as four levels of factor A. The levels of number of blades (B) are selected as 3, 4, 5, and 6.

For the hub radius (C) (the third factor), 0.125, 0.175, 0.150, and 0.200 m are chosen as the levels. Also, for the hub shape (factor D) four different levels (I, II, III, and IV) with four parabola equations are considered in order to test and find the optimum configuration. The selected shapes of hub and their corresponding parabolic equations are shown in Figure 10. The hub shapes vary from a conical shape with equation y=x^0.8 to a hemisphere with equation y=x^0.2.

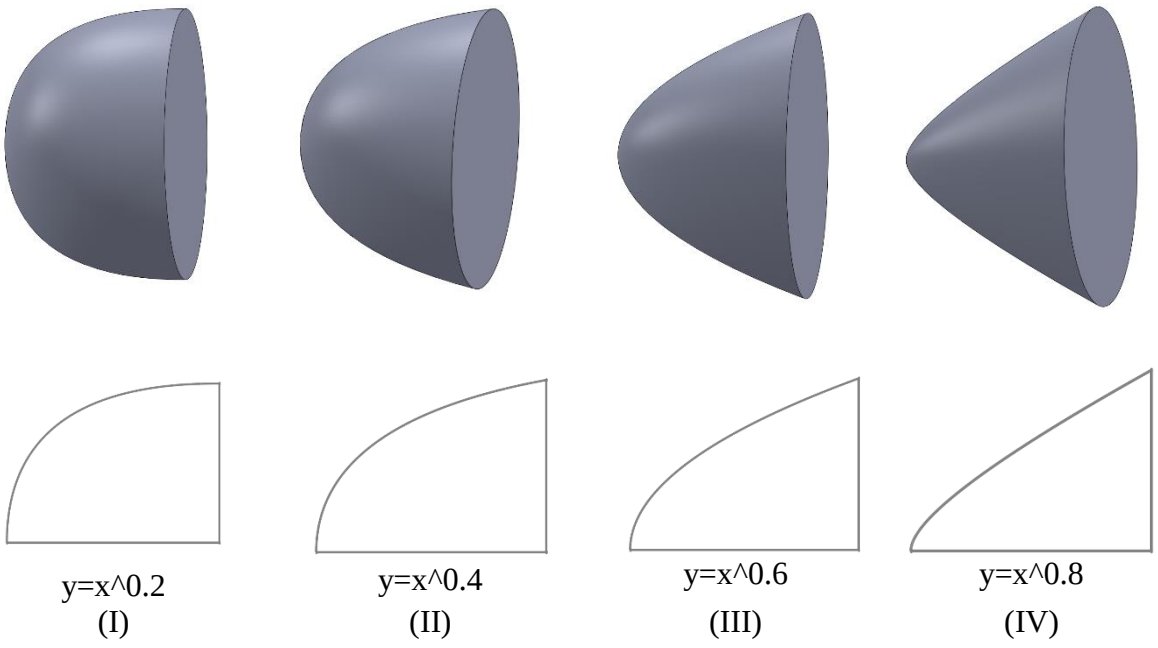

Figure 10. 4 different hub shapes.

All the factors and levels are summarized in Table 3.

Table 3. Specified factors and levels

Factors	Coded levels			
A: Size of blade	0.7b	0.8b	0.9b	1.0b
B: Number of blades	3	4	5	6
C: Hub radius (m)	0.125	0.175	0.150	0.200
D: Hub shape	I	II	III	IV

Stage 3: Orthogonal Array

The Taguchi method employs a structured orthogonal array (OA) in design of experiments. By utilizing structured orthogonal array, the Taguchi method can substantially decrease the number of experiments [86]. The orthogonal array (OA) is a sort of test in which columns are "orthogonal" to each other for the independent factors. The data of the constructed experiment can be examined using both the Taguchi and analysis of variance (ANOVA) methods [87]. According to the previous stage, the OA should be adapted for the four factors at the four-level experiment design. For all identified factors and their levels, the feasible orthogonal array is L16 (4^4) which is built as seen in Table 4. According to Table 4, instead of 256 possible cases (4*4*4*4=256), 16 CFD simulations are evaluated to minimize the geometry of the designed HAT turbine with the four factors, each in four levels.

Table 4. Selected $L_{16}(4^4)$ OA of the set factors and levels

No.	A	B	C	D
Test 1	1	1	1	1
Test 2	1	2	2	2
Test 3	1	3	3	3
Test 4	1	4	4	4
Test 5	2	1	2	3
Test 6	2	2	1	4
Test 7	2	3	4	1
Test 8	2	4	3	2
Test 9	3	1	3	4
Test 10	3	2	4	3
Test 11	3	3	1	2
Test 12	3	4	2	1
Test 13	4	1	4	2
Test 14	4	2	3	1
Test 15	4	3	2	4
Test 16	4	4	1	3

Stage 4: Computational Fluid Dynamics (CFD) analysis

Figure 11 shows the 16 different cases which have been modelled with SOLIDWORKS software, in accordance with the specifications described in Table 3 and the designed orthogonal array (Table 4). As described in stage 1 of the Taguchi method, in this work, power output (P) is used as the objective function (OF). The power output of each case can be measured by torque coefficients (C_m) using Eq. 10. Accordingly, all the torque coefficients at different azimuth angles and TSR=5 are determined from the CFD simulations and the results are plotted in Figure 12.

$$P = 0.5 C_m \rho A_t U_\infty^3 \omega \quad (10)$$

where ω is angular velocity, and A_t is area of the blades.

Figure 12 demonstrates the variations of instantaneous torque coefficient (C_m) in one revolution at TSR=5 for 16 HAT turbine cases as well as the baseline turbine after the steady state condition is attained. The maximum and minimum average torque coefficients (C_m) correspond to cases 4 and 9 which are 0.125 and 0.08 respectively. The value of C_m (0.125) obtained for case 4 is 25% higher than that of the baseline case, which is 0.10.

The power output (P) of each case is calculated using Eq. 10 and the results are presented in Table 5. For example, two of the highest values of power output (4002 and 3600 W, corresponding to deigns 4 and 16 respectively) are related to turbines with 6 blades and the two lowest power outputs (2809 and 2907 W, corresponding to deigns 9 and 13 respectively) are related to 3-blade turbine. Increasing of the number of blades provides greater torque; however, the maximum power output of a turbine must have a finite number of blades [66].

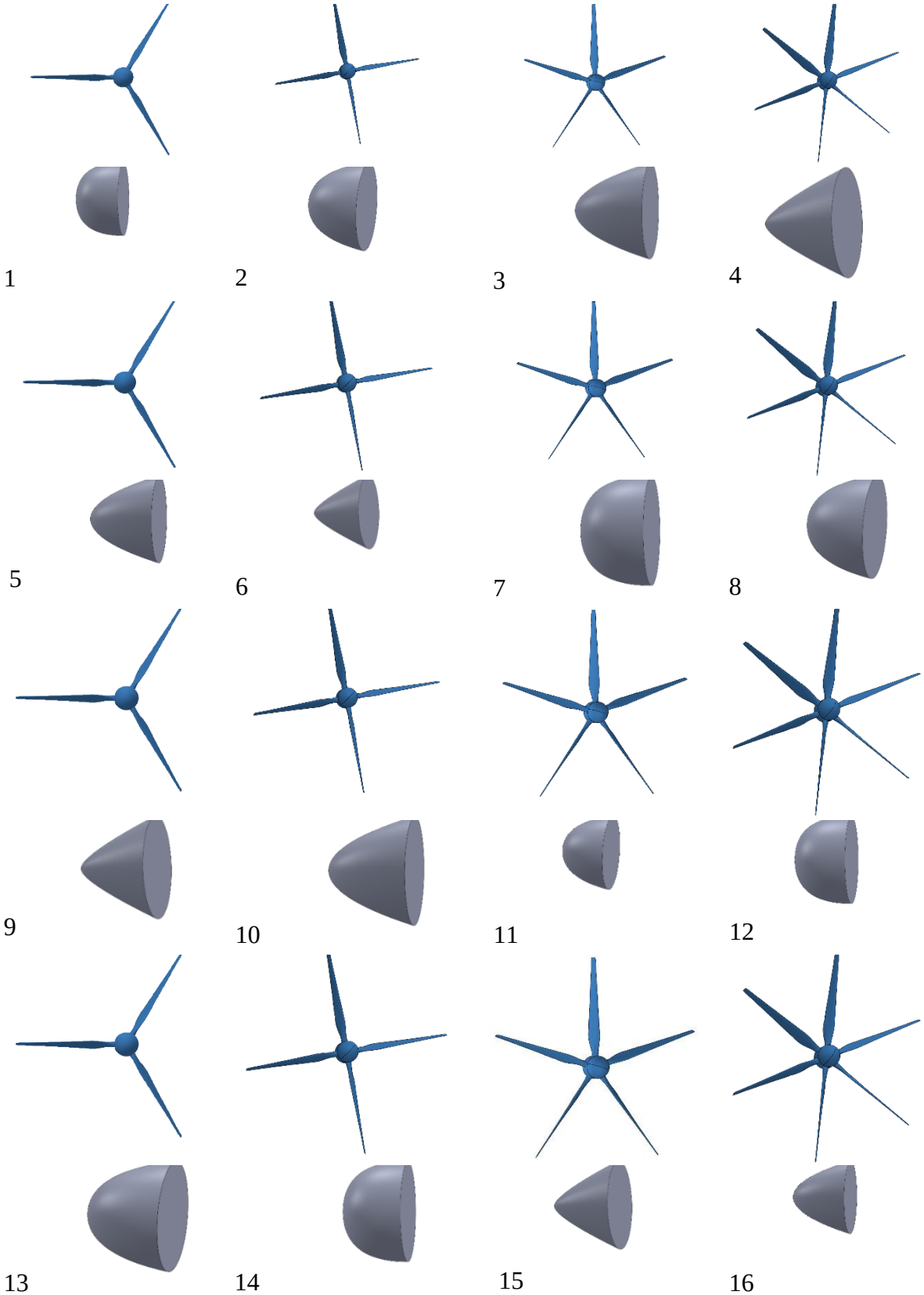

Figure 11. 16 different designs based on L_{16} OA.

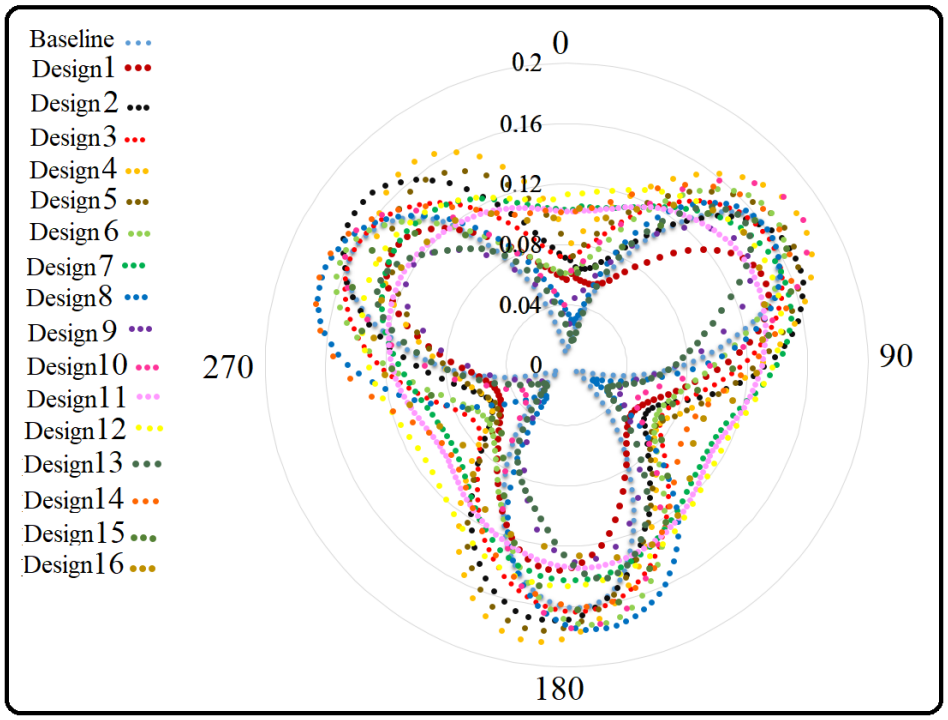

Figure 12. Changes in torque coefficient of all cases for one revolution (0-360º) at TSR=5.

Stage 5: Identification of the optimum factors and their levels

Eq. 8 is used to calculate the SNR of 16 different designs, according to the data shown in Table 3, and the results are presented in Table 4. According to Eq. 8, the smallest value of SNR occurs when there is the smallest difference between the power output and the target quality. From Table 5, it can be seen that the lowest SNR (32) corresponds to design 6, which has the smallest difference between the power output (3476 W) and the target quality (3440 W). The Taguchi method is utilized in the next step to evaluate the order of effect and the optimum combination of the factors to be achieved in the optimized model. For all the factors and their levels, the mean SNR is calculated and the results are plotted in Figure 13. For example, the mean SNR of A1 is

computed from the mean values of all level 1 of factor A [(53+ 43.5+ 39.7+55)/4=47.8]. The results show that power output of the combination A2, B2, C1, and D4 can provide the target quality with smallest geometry. An indicator (β) is determined, as the distance between each factor's top and bottom mean SNRs in Figure 13, to identify the order of influence of all four factors. For variables A, B, C, and D, the values of this indicator are 11.32, 12.2, 6.1 and 5.72 respectively. This clearly indicates that factor B (number of blades) is the main factor amongst all the evaluated factors, influencing the turbine's power output. On the other hand, factors C (hub radius) and D (hub shape) have the smallest effect on hydrodynamic performance of the HAT turbine.

Table 5. L_{16} OA

No.	Size of blade (A)	Number of blades (B)	Hub radius (C)	Hub shape (D)	P (W)	SNR
Baseline	b	3	0.200	III	3417	N/A
Test 1	0.7b	3	0.125	I	2993	53
Test 2	0.7b	4	0.150	II	3589	43.5
Test 3	0.7b	5	0.175	III	3536	39.7
Test 4	0.7b	6	0.200	IV	4002	55
Test 5	0.8b	3	0.150	III	3537	39.8
Test 6	**0.8b**	**4**	**0.125**	**IV**	**3479**	**32**
Test 7	0.8b	5	0.200	I	3338	40.1
Test 8	0.8b	6	0.175	II	3490	34
Test 9	0.9b	3	0.175	IV	2809	56
Test 10	0.9b	4	0.200	III	3298	43
Test 11	0.9b	5	0.125	II	3349	39.1
Test 12	0.9b	6	0.150	I	3589	43.5
Test 13	1.0b	3	0.200	II	2907	54.5
Test 14	1.0b	4	0.175	I	2998	52.9
Test 15	1.0b	5	0.150	IV	3500	35.6
Test 16	1.0b	6	0.125	III	3600	44.1

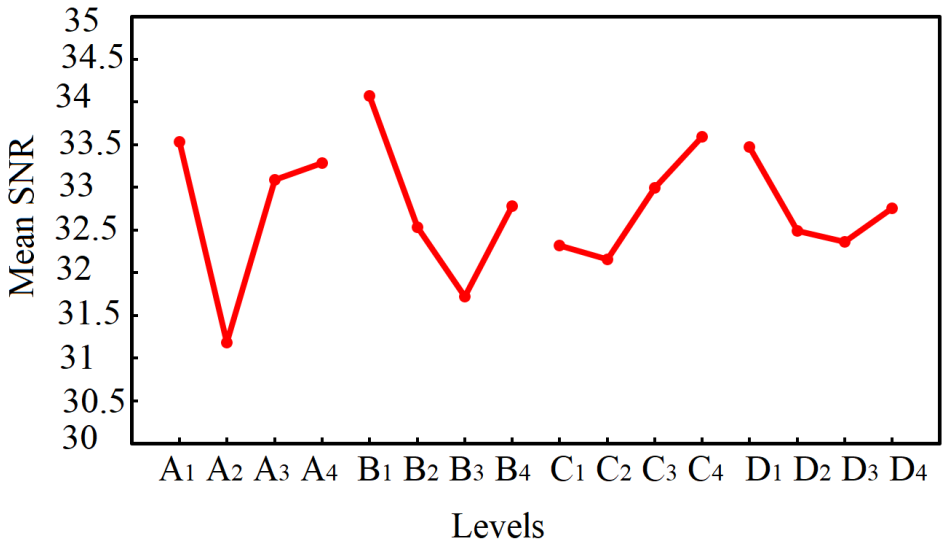

Figure 13. Mean SNR (smaller is the better) for different factors and levels.

Stage 6: Analysis of Variance (ANOVA)

In this stage, the interaction of all factors and with their levels is analyzed by using ANOVA. The objective of ANOVA analysis is to evaluate the interaction between factors with respect to the overall variation of all variables. There are different classical approaches for ANOVA analysis for unbalanced data. In this paper, two-way interaction is used. In general, the difference between two-way, three-way, and four-way interaction is negligible and most of the relevant literature have used two-way interaction [88-90]. The relationship plot of ANOVA can be used to display the interaction between the factors in different levels [91, 92]. According to the obtained interaction plots, two different potential options (a: parallel and b: non-parallel) can be considered (Figure 14). In parallel patterns, a certain interaction will not happen and can be ignored, whilst the interaction in non-parallel trends is important and should be considered. By using the SNRs listed in Table 5, the relationship between each of two variables is measured and presented in Figure 15 [34, 35].

In the interpretation of ANOVA interaction plots, when interaction exists amongst the factors, the lines will be non-parallel [92]. By assessing the obtained ANOVA interaction plots (Figure 15), it can be seen that there is an interaction between each pair of factors due to non-parallel lines. Between the assessed variables, the interaction between number of blades (factor B) and other factors is very strong due to the number of non-parallel lines in comparison to other interactions. This is also highlighted in the results of the Taguchi method, where factor B has the greatest effect on the power output of the HAT turbine (stage 5).

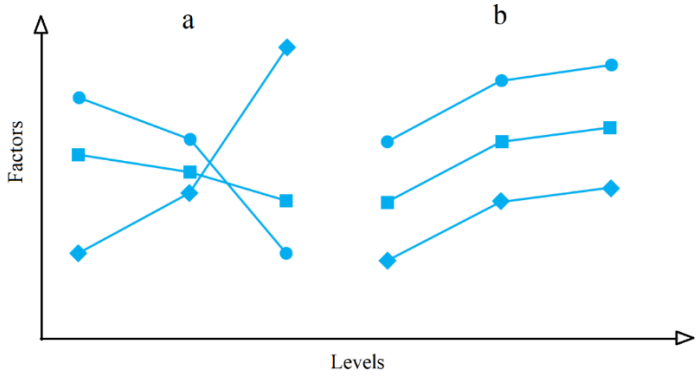

Figure 14. (a) Interaction and (b) no interaction graphs for analysis of variance [92].

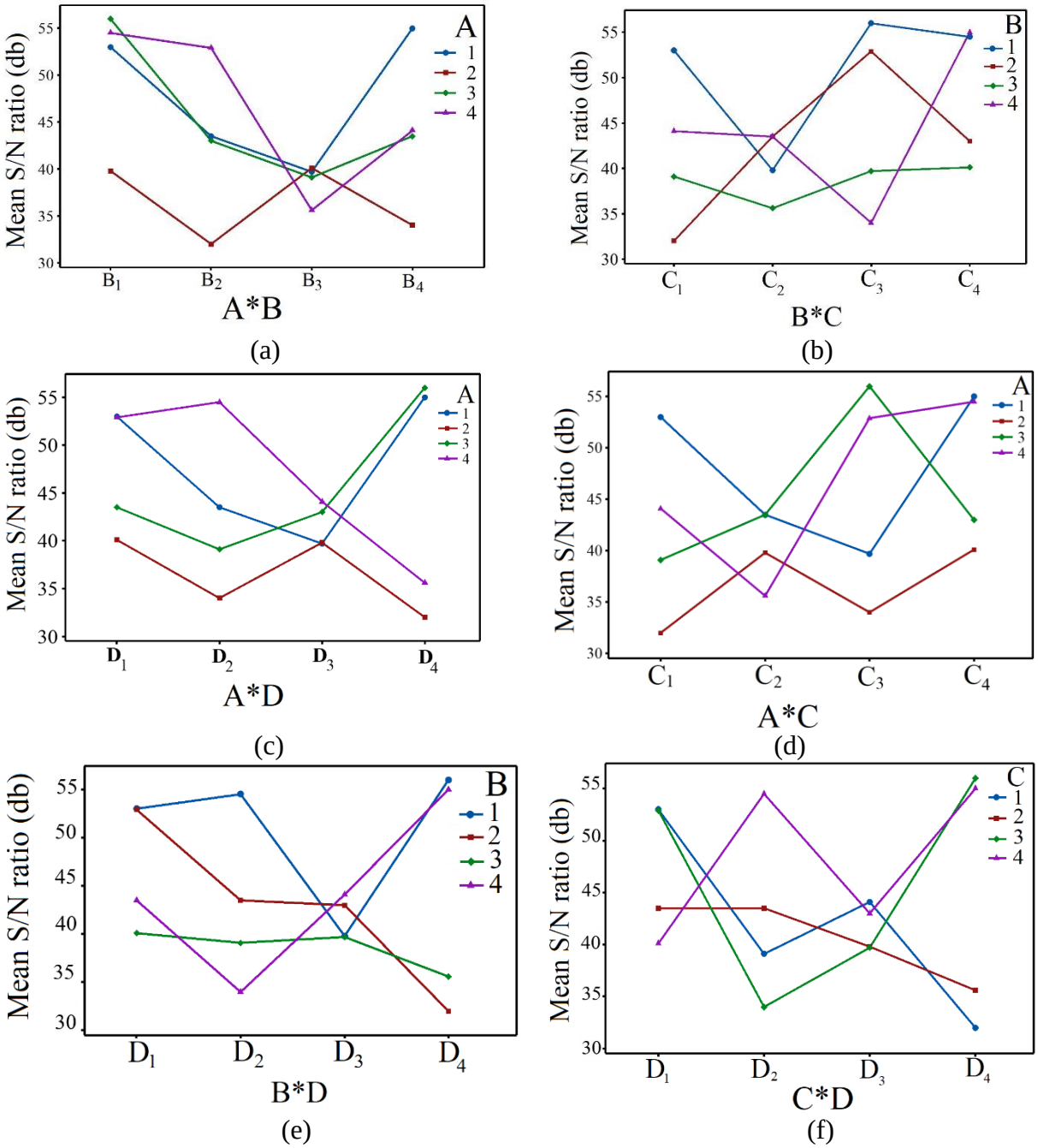

Figure 15. Interaction graphs for analysis of variance.

476

477

478

479

Stage 7: Superposition model

The superposition model sues SNRs, which are obtained from the Taguchi method, to estimate all possible ratios outside the orthogonal array. In this study, the superposition model (according to [35]) is used to predict the SNRs of all responses (4*4*4*4= 256). Considering the percentage of errors is close to zero and can be neglected [34], the superposition model for the four-level four-factor problem will be:

$$\psi^t(A_i, B_j, C_k, D_l) = \psi + (\psi_{Ai} - \psi) + (\psi_{Bj} - \psi) + (\psi_{Ck} - \psi) + (\psi_{Dl} - \psi) \quad (11)$$

where ψ^t is the predicted SNR, ψ is the mean of total mean SNRs, ψ_{Ai} is the mean SNRs of factor A at level i, $\psi_{Bj}$is the mean SNRs of factor B at level j, $\psi_{Ck}$is the mean SNRs of factor C at level k, and ψ_{Dl} is the mean SNRs of factor D at level l.

The obtained equation is solved using MATLAB software and the results are shown in Table 6. It can be seen from this table that the lowest SNR is for case 103 and its value is 25.01. This value is for combination of factors A2, B3, C2, and D3. The obtained SNR value for the combination A2, B3, C2, and D3 is almost 21% less than the amount obtained in the Taguchi method (case 6, SNR=32). In should be noted that in Table 6, the SNR value for the obtained combination by the Taguchi method (A2, B2, C1, and D4) is calculated as 33.68, which is more than the minimum value of the Table. Therefore, combination of factors A2, B3, C2, and D3 that is provided by the superposition model, is used to build a HAT turbine as the final optimized model and it is simulated using the CFD method described in section 4.

Table 6. Prediction of signal-to-noise (SNR) of all achievable combinations

No.	A	B	C	D	SNR	NO.	A	B	C	D	SNR	No.	A	B	C	D	SNR	No.	A	B	C	D	SNR
1	1	1	1	1	55.71	65	2	1	1	1	44.38	129	3	1	1	1	53.31	193	4	1	1	1	54.68
2	1	1	1	2	51.11	66	2	1	1	2	39.78	130	3	1	1	2	48.71	194	4	1	1	2	50.08
3	1	1	1	3	49.98	67	2	1	1	3	38.66	131	3	1	1	3	47.58	195	4	1	1	3	48.96
4	1	1	1	4	52.98	68	2	1	1	4	41.66	132	3	1	1	4	50.58	196	4	1	1	4	51.96
5	1	1	2	1	54.26	69	2	1	2	1	42.93	133	3	1	2	1	51.86	197	4	1	2	1	53.23
6	1	1	2	2	49.66	70	2	1	2	2	38.33	134	3	1	2	2	47.26	198	4	1	2	2	48.63
7	1	1	2	3	48.53	71	2	1	2	3	37.21	135	3	1	2	3	46.13	199	4	1	2	3	47.51
8	1	1	2	4	51.53	72	2	1	2	4	40.21	136	3	1	2	4	49.13	200	4	1	2	4	50.51
9	1	1	3	1	59.31	73	2	1	3	1	47.98	137	3	1	3	1	56.91	201	4	1	3	1	58.28
10	1	1	3	2	54.71	74	2	1	3	2	43.38	138	3	1	3	2	52.31	202	4	1	3	2	53.68
11	1	1	3	3	53.58	75	2	1	3	3	42.26	139	3	1	3	3	51.18	203	4	1	3	3	52.56
12	1	1	3	4	56.58	76	2	1	3	4	45.26	140	3	1	3	4	54.18	204	4	1	3	4	55.56
13	1	1	4	1	61.81	77	2	1	4	1	50.48	141	3	1	4	1	59.41	205	4	1	4	1	60.78
14	1	1	4	2	57.21	78	2	1	4	2	45.88	142	3	1	4	2	54.81	206	4	1	4	2	56.18
15	1	1	4	3	56.08	79	2	1	4	3	44.76	143	3	1	4	3	53.68	207	4	1	4	3	55.06
16	1	1	4	4	59.08	80	2	1	4	4	47.76	144	3	1	4	4	56.68	208	4	1	4	4	58.06
17	1	2	1	1	47.73	81	2	2	1	1	36.41	145	3	2	1	1	45.33	209	4	2	1	1	46.71
18	1	2	1	2	43.13	82	2	2	1	2	31.81	146	3	2	1	2	40.73	210	4	2	1	2	42.11
19	1	2	1	3	42.01	83	2	2	1	3	30.68	147	3	2	1	3	39.61	211	4	2	1	3	40.98
20	1	2	1	4	45.01	**84**	**2**	**2**	**1**	**4**	**33.68**	148	3	2	1	4	42.61	212	4	2	1	4	43.98
21	1	2	2	1	46.28	85	2	2	2	1	34.96	149	3	2	2	1	43.88	213	4	2	2	1	45.26
22	1	2	2	2	41.68	86	2	2	2	2	30.36	150	3	2	2	2	39.28	214	4	2	2	2	40.66
23	1	2	2	3	40.56	87	2	2	2	3	29.23	151	3	2	2	3	38.16	215	4	2	2	3	39.53
24	1	2	2	4	43.56	88	2	2	2	4	32.23	152	3	2	2	4	41.16	216	4	2	2	4	42.53
25	1	2	3	1	51.33	89	2	2	3	1	40.01	153	3	2	3	1	48.93	217	4	2	3	1	50.31
26	1	2	3	2	46.73	90	2	2	3	2	35.41	154	3	2	3	2	44.33	218	4	2	3	2	45.71
27	1	2	3	3	45.61	91	2	2	3	3	34.28	155	3	2	3	3	43.21	219	4	2	3	3	44.58
28	1	2	3	4	48.61	92	2	2	3	4	37.28	156	3	2	3	4	46.21	220	4	2	3	4	47.58
29	1	2	4	1	53.83	93	2	2	4	1	42.51	157	3	2	4	1	51.43	221	4	2	4	1	52.81
30	1	2	4	2	49.23	94	2	2	4	2	37.91	158	3	2	4	2	46.83	222	4	2	4	2	48.21
31	1	2	4	3	48.11	95	2	2	4	3	36.78	159	3	2	4	3	45.71	223	4	2	4	3	47.08
32	1	2	4	4	51.11	96	2	2	4	4	39.78	160	3	2	4	4	48.71	224	4	2	4	4	50.08
33	1	3	1	1	43.51	97	2	3	1	1	32.18	161	3	3	1	1	41.11	225	4	3	1	1	42.48
34	1	3	1	2	38.91	98	2	3	1	2	27.58	162	3	3	1	2	36.51	226	4	3	1	2	37.88
35	1	3	1	3	37.78	99	2	3	1	3	26.46	163	3	3	1	3	35.38	227	4	3	1	3	36.76
36	1	3	1	4	40.78	100	2	3	1	4	29.46	164	3	3	1	4	38.38	228	4	3	1	4	39.76
37	1	3	2	1	42.06	101	2	3	2	1	30.73	165	3	3	2	1	39.66	229	4	3	2	1	41.03
38	1	3	2	2	37.46	102	2	3	2	2	26.13	166	3	3	2	2	35.06	230	4	3	2	2	36.43
39	1	3	2	3	36.33	**103**	**2**	**3**	**2**	**3**	**25.01**	167	3	3	2	3	33.93	231	4	3	2	3	35.31
40	1	3	2	4	39.33	104	2	3	2	4	28.01	168	3	3	2	4	36.93	232	4	3	2	4	38.31
41	1	3	3	1	47.11	105	2	3	3	1	35.78	169	3	3	3	1	44.71	233	4	3	3	1	46.08
42	1	3	3	2	42.51	106	2	3	3	2	31.18	170	3	3	3	2	40.11	234	4	3	3	2	41.48
43	1	3	3	3	41.38	107	2	3	3	3	30.06	171	3	3	3	3	38.98	235	4	3	3	3	40.36
44	1	3	3	4	44.38	108	2	3	3	4	33.06	172	3	3	3	4	41.98	236	4	3	3	4	43.36
45	1	3	4	1	49.61	109	2	3	4	1	38.28	173	3	3	4	1	47.21	237	4	3	4	1	48.58
46	1	3	4	2	45.01	110	2	3	4	2	33.68	174	3	3	4	2	42.61	238	4	3	4	2	43.98
47	1	3	4	3	43.88	111	2	3	4	3	32.56	175	3	3	4	3	41.48	239	4	3	4	3	42.86
48	1	3	4	4	46.88	112	2	3	4	4	35.56	176	3	3	4	4	44.48	240	4	3	4	4	45.86
49	1	4	1	1	49.03	113	2	4	1	1	37.71	177	3	4	1	1	46.63	241	4	4	1	1	48.01
50	1	4	1	2	44.43	114	2	4	1	2	33.11	178	3	4	1	2	42.03	242	4	4	1	2	43.41
51	1	4	1	3	43.31	115	2	4	1	3	31.98	179	3	4	1	3	40.91	243	4	4	1	3	42.28
52	1	4	1	4	46.31	116	2	4	1	4	34.98	180	3	4	1	4	43.91	244	4	4	1	4	45.28
53	1	4	2	1	47.58	117	2	4	2	1	36.26	181	3	4	2	1	45.18	245	4	4	2	1	46.56
54	1	4	2	2	42.98	118	2	4	2	2	31.66	182	3	4	2	2	40.58	246	4	4	2	2	41.96
55	1	4	2	3	41.86	119	2	4	2	3	30.53	183	3	4	2	3	39.46	247	4	4	2	3	40.83
56	1	4	2	4	44.86	120	2	4	2	4	33.53	184	3	4	2	4	42.46	248	4	4	2	4	43.83
57	1	4	3	1	52.63	121	2	4	3	1	41.31	185	3	4	3	1	50.23	249	4	4	3	1	51.61
58	1	4	3	2	48.03	122	2	4	3	2	36.71	186	3	4	3	2	45.63	250	4	4	3	2	47.01
59	1	4	3	3	46.91	123	2	4	3	3	35.58	187	3	4	3	3	44.51	251	4	4	3	3	45.88
60	1	4	3	4	49.91	124	2	4	3	4	38.58	188	3	4	3	4	47.51	252	4	4	3	4	48.88
61	1	4	4	1	55.13	125	2	4	4	1	43.81	189	3	4	4	1	52.73	253	4	4	4	1	54.11
62	1	4	4	2	50.53	126	2	4	4	2	39.21	190	3	4	4	2	48.13	254	4	4	4	2	49.51
63	1	4	4	3	49.41	127	2	4	4	3	38.08	191	3	4	4	3	47.01	255	4	4	4	3	48.38
64	1	4	4	4	52.41	128	2	4	4	4	41.08	192	3	4	4	4	50.01	256	4	4	4	4	51.38

501

502

6. Fluid dynamics study

With the combinations obtained from the superposition model and Table 3, the optimized turbine is designed in SOLIDWORKS 2017. The initial SOLIDWORKS design shows that the weight of optimized design is 17% less than the baseline design; hence it requires less material and can be manufactured cheaper. A comprehensive CFD simulation of the baseline and the optimized designs is carried out using ANSYS Fluent 2019 (as described in section 2) and the results are presented in this section. Using Eq. 10 and the CFD results, the power output of the optimized turbine is calculated to be 3830 W, which is suitable for the mentioned desalination system to produce 1 m^3/h freshwater (see section 2.4).

Figure 16 shows a comparison of the variations of power coefficient (C_p) with TSR for the baseline and optimized HAT turbines. When comparing the performance of the presented HAT turbines at various tip speed ratios (TSRs), the change of the blade size and number of blades helps to increase the power coefficient (C_p), however, after a particular TSR, the power output of the turbines decreases due to the increased turbulence. According to the obtained results, at TSR=5, C_p of the optimized model is 0.44, while for the baseline design it is 0.40 (it is 10% more for the optimized model). Moreover, the optimized 5-blade HAT turbine performs better at lower TSR (3-5.5) and the baseline 3-blade HAT turbine works better at higher TSR (5.5-6.5). To further investigate this, it is necessary to simulate both turbines at different TSRs. Figure 17 shows the streamline contours across the revolving turbine in four different tip speed ratios (TSRs). The contour plots explicitly illustrate that the velocity deficiency is dependent on the TSRs which are provided by different inlet velocities. The water rotates the HAT turbine and the passing stream rotates in an inverse direction of the turbine. While water moves through the turbine, the turbine absorbs the energy of the water and hence there is a difference in the velocity of the upstream and downstream. The

higher the inlet velocity, the greater is the difference in velocity. In both turbines, the flow runs normally at low TSRs and from upstream to downstream. In the baseline turbine, according to Figure 17, there is a heavy turbulence in the streamline distributions when the TSR changes from 5.5 to 6.0. However, in the optimized turbine this occurs after TSR=5.0 and the streamlines of downstream face a huge turbulence. These results provide further evidence for the findings in Figure 16, which show the optimized turbine has better performance at lower TSRs.

The vorticity contours of the CFD simulations of both turbines through a cross section (YZ plane) at azimuth angles of 40°, 80°, and 120° are presented in Figure 18. For these contours to be comparable, one of the turbine blades is marked with letter Q (indicator blade) and the value of azimuth angle is defined according to this indicator blade. The results show that the (three-blade) baseline turbine experiences greater vortex and wake in comparison with the optimized (five-blade) turbine, which results in better performance. The vorticity is indeed greater on the top of the blades due to rotational impact of the turbine blades, and the velocity gradient is much wider. The lower magnitude of vorticity at the bottom of the blades can be attributed to the separation of the flow on the blade surface, and it is very visible at the proximity of turbine hub. For both turbines, the energy contribution of blades near the hub is less than the section near the tip portion. The CFD simulation in ANSYS Fluent considers the solid parts as rigid body and it does not consider the deformation and vibration. However, in reality, the increase in the vortex at the end of the turbine blades causes an increase in vibration as well as deformation, which reduces the lifetime and the efficiency of the turbine. This further confirms the superiority of the optimized turbine, which has smaller blades (20% smaller) than the baseline turbine.

Finally, to better understand and compare the effect of different hubs on hydrodynamic performance of the HAT turbines, the velocity contours at three different azimuth angles on the

ZX plane are shown in Figure 19. All contours are plotted at TSR of 5.0. As can be seen from this Figure, type III hub, which is used in the optimized model (compared to the type I (baseline model)), can be used to suppress the flow separation at different azimuth angles. On the other hand, in the baseline model, after water hits the nose of the hub, it causes separation and turbulence immediately, which can reduce the kinetic energy of water and the efficiency of the turbine. It can be concluded that the combination of the number of turbine blades and the type of hub can affect the performance of the turbine, as predicted in the previous section by the ANOVA method.

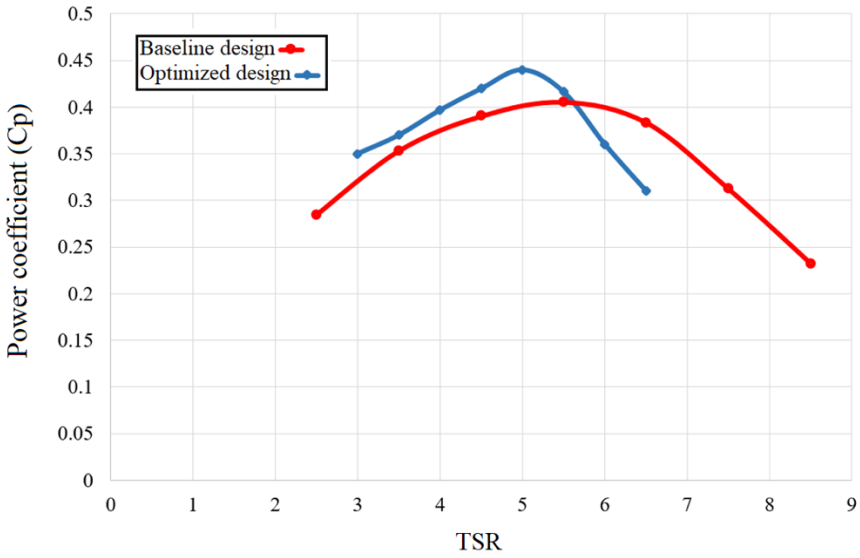

Figure 16. Variation of power coefficient (C_p) with tip speed ratio (TSR) of baseline and optimized designs

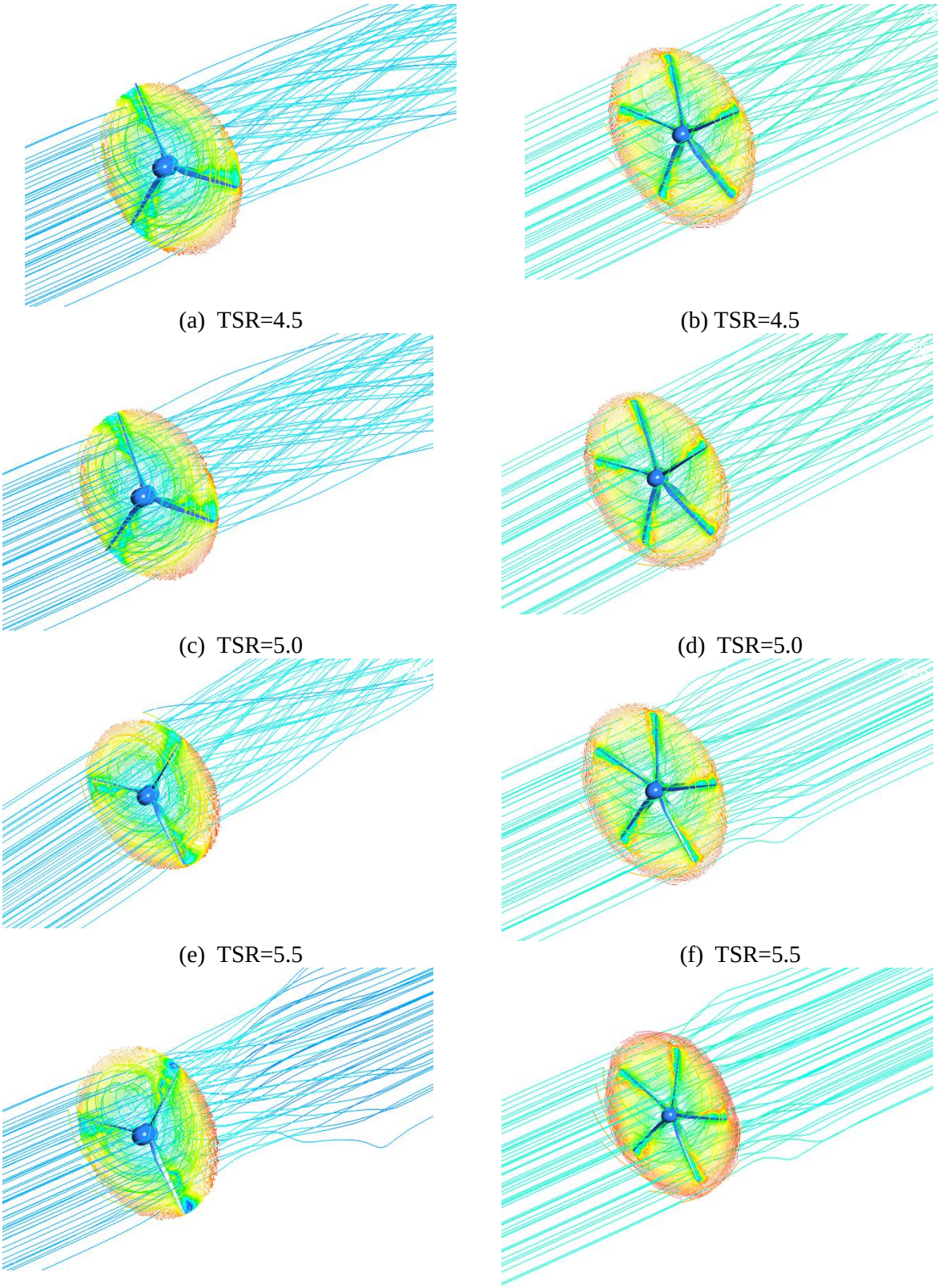

(a) TSR=4.5 (b) TSR=4.5

(c) TSR=5.0 (d) TSR=5.0

(e) TSR=5.5 (f) TSR=5.5

(g) TSR=6.0 (h) TSR=6.0

Figure 17. Streamline distributions in 4 different tip speed ratios (TSR).

560

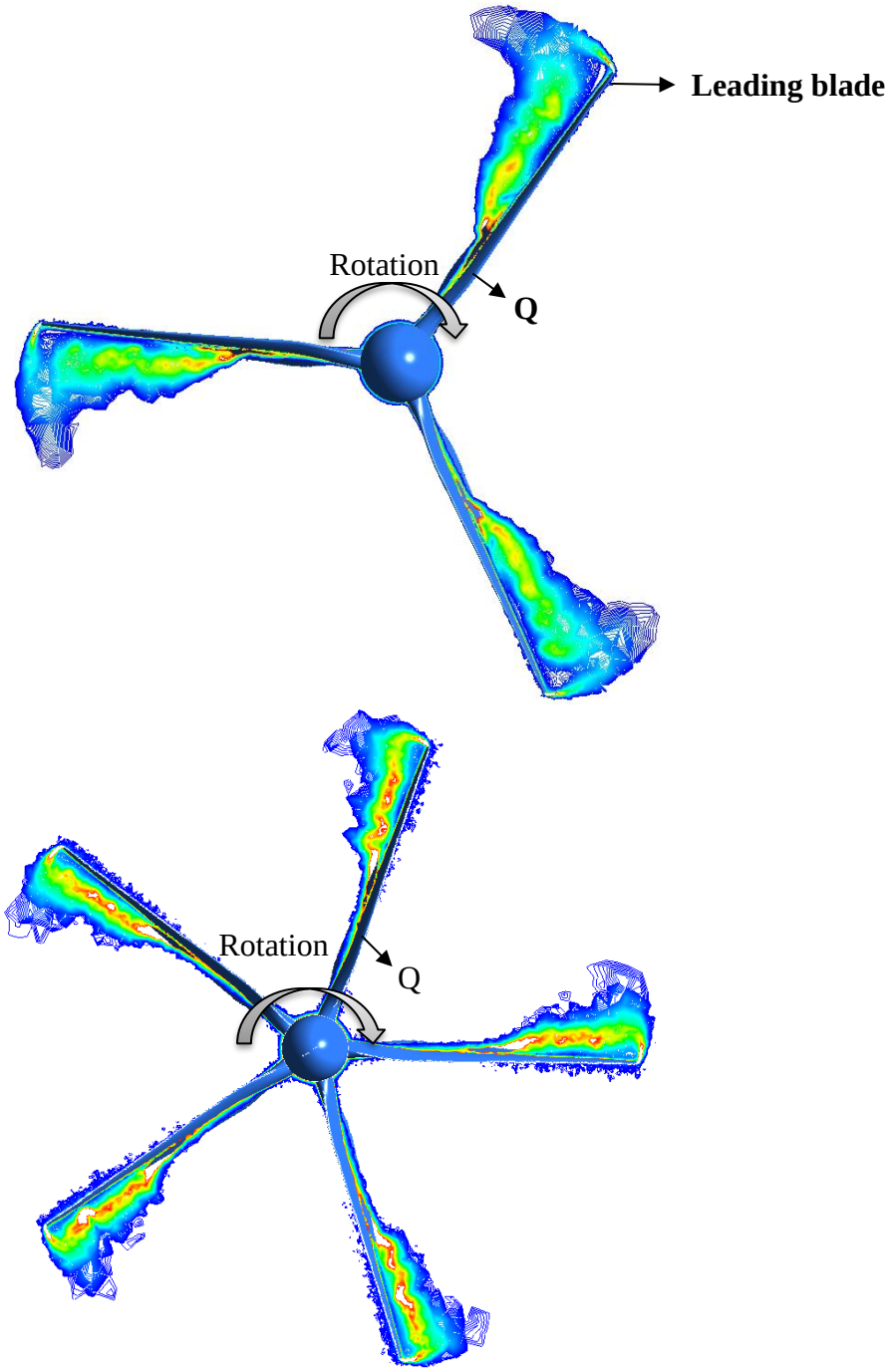

Azimuth angle: 40^{o}

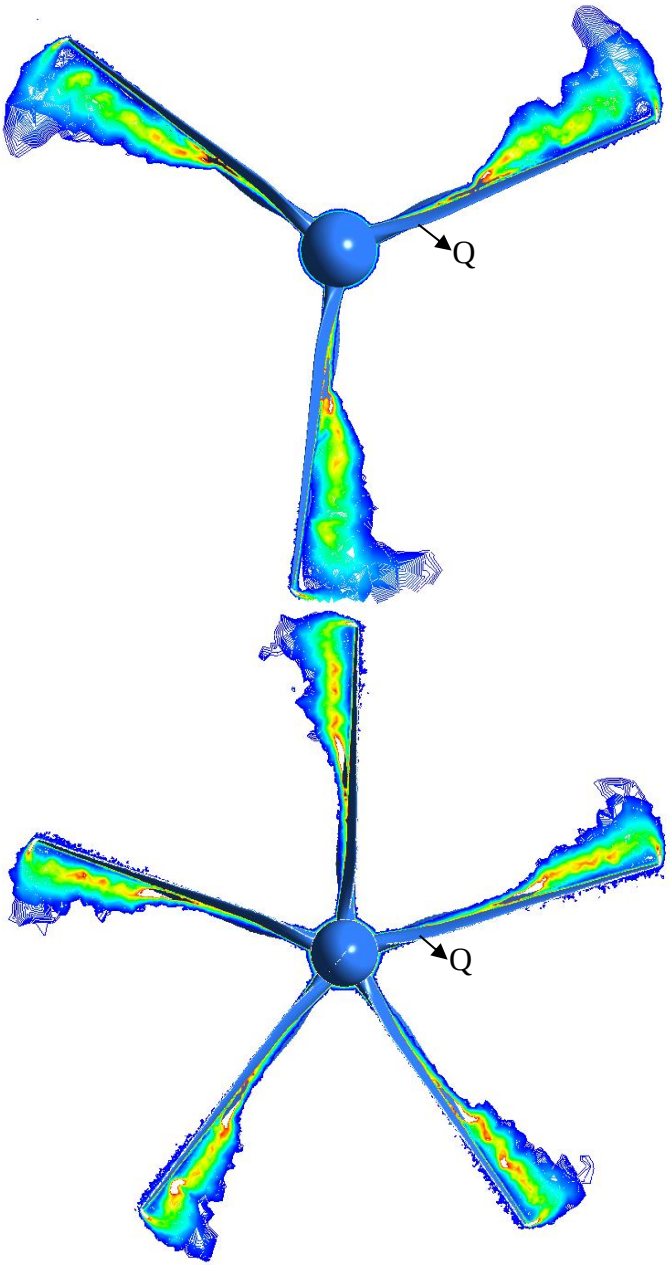

Azimuth angle: 80º

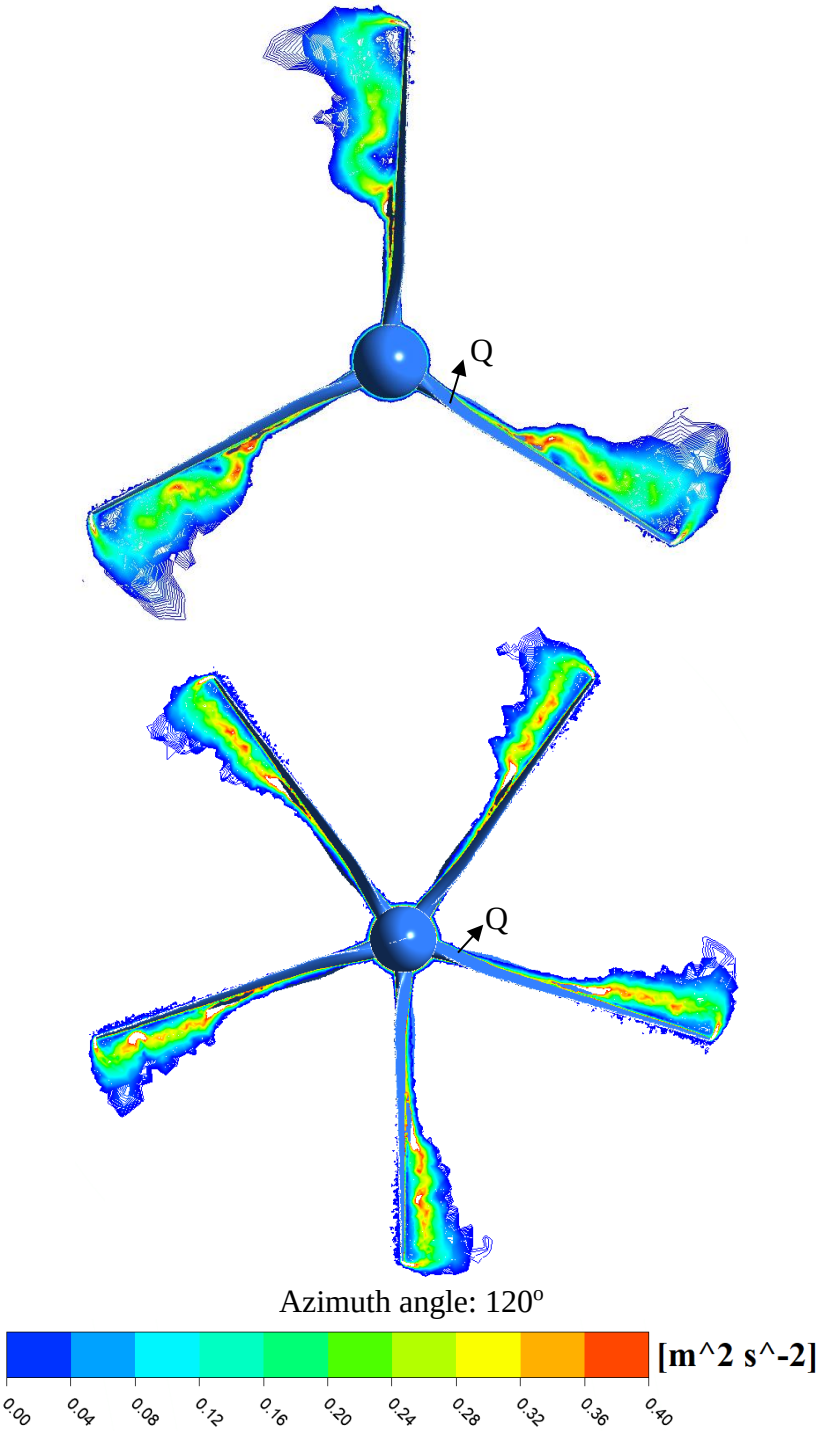

Figure 18. Vorticity contours at different azimuth angles.

561

562

563

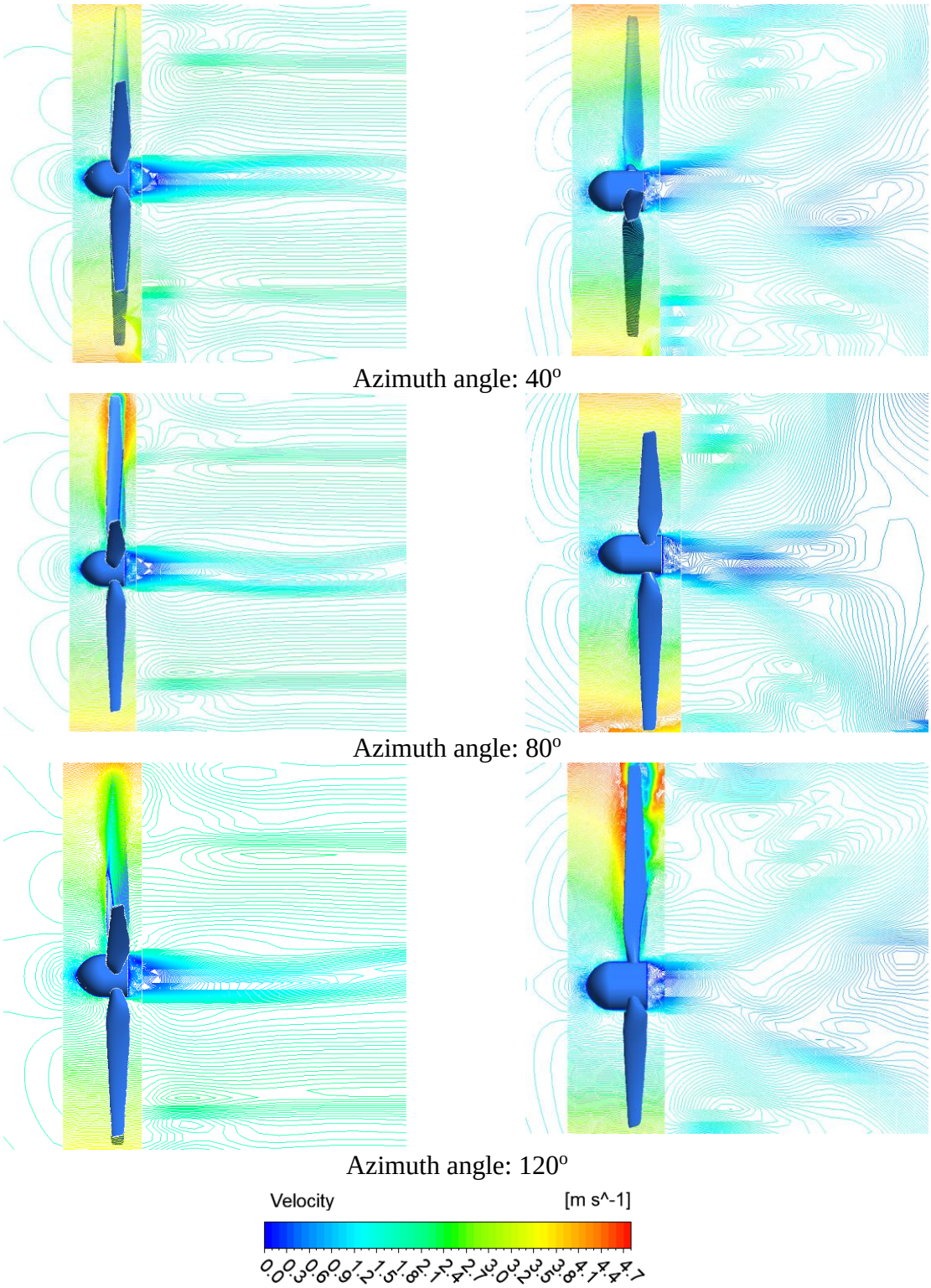

Figure 19. Velocity distribution at different azimuth angles (left: optimized model and right: baseline model).

564

7. Conclusion

The Taguchi method and extensive CFD simulations were utilized in this study to minimize the geometry of a HAT turbine, designed to power a desalination system. The results show that the Taguchi method is an effective tool for optimization of complex HAT turbines by using only few experiments. The main conclusions of this paper can be summarized as follows:

(1) The optimum combination of the tested factors by the Taguchi method was achieved as (design 6): size of blade: 0.8b; number of blades: 4; hub radius: 0.125 m; and hub shape: type IV. The β indicator of variables A, B, C, and D, was calculated as 11.32, 12.2, 6.1 and 5.72 respectively. This indicates that number of blades (B) is the main influential factor among the four assessed factors. The hub radius (C) and hub shape (D) have the least influence on the HAT turbine's hydrodynamic output.

(2) The results from ANOVA analysis showed that all four parametric variables have vivid interactions with each other. Among the analyzed factors, the interaction of the number of blades (B) and other variables was stronger.

(3) The results of the superposition model showed that the minimum SNR was 25.01 for design 103, which was 21% less than the value achieved in the Taguchi approach. This value was for the combination of size of blade: 0.8b; number of blades: 5; hub radius: 0.150 m; and hub shape: type III. The weight of optimized model was 17% less than the baseline model, indicating that the optimized model would require less material and can be made cheaper.

(4) According to the CFD simulations, C_p of the optimized model was 0.44, which was 10% higher than the baseline model (0.40) at tip speed ratio (TSR) of 5. The optimized HAT turbine works

better at lower TSR (3-5.5) and the baseline HAT turbine performs better at higher TSR (5.5-6.5).

The impacts of deformation of the HAT turbine were not considered in this study. In addition, the efficiency of a HAT turbine is affected by the roughness of the turbine blades, which can be considered as a variable in the Taguchi approach, and its individual effects can be studied and compared with other variables. Moreover, an economic analysis of HAT turbines based on different materials is a potential area for future work.

Declaration of Competing Interest

The authors declare that they have no known competing financial interests or personal relationships that could have appeared to influence the work reported in this paper.

Acknowledgement

The authors would like to acknowledge the financial support from the College of Engineering, Mathematics and Physical Sciences of the University of Exeter for this project.

References

1. Xu J., Wang Z., Chang C., Fu B., Tao P., Song C., Shang W., and Deng T., *Solar-driven interfacial desalination for simultaneous freshwater and salt generation.* Desalination, 2020. **484**: p. 114423.
2. Shannon M. A., Bohn P. W., Elimelech M., Georgiadis J. G., Marinas B. J., and Mayes A. M., *Science and technology for water purification in the coming decades*. *Nanoscience and technology: a collection of reviews from nature Journals*. 2010, World Scientific. p. 337-346.
3. FAO UN-Water, *Coping with Water Scarcity: Challenge of the Twenty-First Century (2007)*.
4. Van Dam J. C., *Impacts of climate change and climate variability on hydrological regimes*. 2003: Cambridge University Press.
5. Boorman D., Dumont E., Houghton-Carr H., Jenkins A., Keller V., Miller J., Hughes A., Majdi M., Mackay J., *WATER SECURITY IN THE UK, A pilot model-based study of*

current and future water security in the UK. 2012: Natural Environment Research Council.
6. Thompson S. A., *Hydrology for water management*. 2017: CRC Press.
7. El-Ghonemy A., *Retracted: water desalination systems powered by renewable energy sources, Review*. 2012, Elsevier.
8. Laborde H., Franca K., Neff H., and Lima A., *Optimization strategy for a small-scale reverse osmosis water desalination system based on solar energy.* Desalination, 2001. **133**(1): p. 1-12.
9. Han D., He W., Yue C., and Pu W., *Study on desalination of zero-emission system based on mechanical vapor compression.* Applied energy, 2017. **185**: p. 1490-1496.
10. Ang W. L., Mohammad A. Hilal W., N. and C. P. Leo, *A review on the applicability of integrated/hybrid membrane processes in water treatment and desalination plants.* Desalination, 2015. **363**: p. 2-18.
11. Peñate B. and García-Rodríguez L ., *Current trends and future prospects in the design of seawater reverse osmosis desalination technology.* Desalination, 2012. **284**: p. 1-8.
12. Tong X., Liu S., Chen Y., and Crittenden J., *Thermodynamic analysis of a solar thermal facilitated membrane seawater desalination process.* Journal of Cleaner Production, 2020. **256**: p. 120398.
13. Turek M. and B. Bandura, *Renewable energy by reverse electrodialysis.* Desalination, 2007. **205**(1-3): p. 67-74.
14. Tzen E. and Morris R., *Renewable energy sources for desalination.* Solar energy, 2003. **75**(5): p. 375-379.
15. Pelc R. and Fujita R.M., *Renewable energy from the ocean.* Marine Policy, 2002. **26**(6): p. 471-479.
16. Nadel B., *Portable sea-powered electrolysis generator*. 2008, Google Patents.
17. Amy G., Ghaffour N., Li Z., Francis L., Linares R. V., Missimer T., and Lattemann S., *Membrane-based seawater desalination: Present and future prospects.* Desalination, 2017. **401**: p. 16-21.
18. Chen D., *Tidal energy seawater desalination system, power generation system and integral energy utilization system*. 2015, Google Patents.
19. Ng K.C. and Shahzad M.W., *Sustainable desalination using ocean thermocline energy.* Renewable and Sustainable Energy Reviews, 2018. **82**: p. 240-246.
20. Khanjanpour M., Javadi A. A., and Akrami M., *CFD analyses of a tidal hydro-turbine (THT) for utilising in sea water desalination.* 2019.
21. Davies P., *Wave-powered desalination: resource assessment and review of technology.* Desalination, 2005. **186**(1-3): p. 97-109.
22. Leijon J., Forslund J., Thomas K., and Boström C., *Marine Current Energy Converters to Power a Reverse Osmosis Desalination Plant.* Energies, 2018. **11**(11): p. 2880.
23. Zhao K. and Y. Liu, *Theoretical study on multi-effect solar distillation system driven by tidal energy.* Desalination, 2009. **249**(2): p. 566-570.
24. Sharmila N., Jalihal P., Swamy A., and Ravindran M., *Wave powered desalination system.* Energy, 2004. **29**(11): p. 1659-1672.
25. Ullman P.W., *Offshore Tidal Power Generation—A new approach to power conversion of the oceans' tides.* Marine Technology Society Journal, 2002. **36**(4): p. 16-24.

26. Ling C., Wang Y., Min C., and Zhang Y., *Economic evaluation of reverse osmosis desalination system coupled with tidal energy.* Frontiers in Energy, 2018. **12**(2): p. 297-304.
27. Ahmadi M. H. and Yang Z., *The evolution of turbulence characteristics in the wake of a horizontal axis tidal stream turbine.* Renewable Energy, 2019.
28. Bouhal T., Rajad O., Kousksou T., Arid A., El Rhafiki T., Jamil A., and Benbassou A., *CFD performance enhancement of a low cut-in speed current Vertical Tidal Turbine through the nested hybridization of Savonius and Darrieus.* Energy conversion and management, 2018. **169**: p. 266-278.
29. Hong Y.Y. and Satriani T. R. A., *Day-ahead spatiotemporal wind speed forecasting using robust design-based deep learning neural network.* Energy, 2020: p. 118441.
30. Jahanshahi M., Sanati M., and Babaei Z., *Optimization of parameters for the fabrication of gelatin nanoparticles by the Taguchi robust design method.* Journal of Applied Statistics, 2008. **35**(12): p. 1345-1353.
31. Sapakal S. and Telsang M., *Parametric optimization of MIG welding using Taguchi design method.* Int J Adv Eng Res Stud, 2012. **1**(4): p. 28-30.
32. Chan L. C., Akrami M., Javadi A. A., G. Tabor, Dibaj M., and Khanjanpour M. H., *Optimisation of a conceptual aircraft model using a genetic algorithm and 3D Computational Fluid Dynamics (CFD).* 2019.
33. Li W. Z., Yang W. W., Wang N., Jiao Y. H., Yang Y., and Qu Z. G., *Optimization of blocked channel design for a proton exchange membrane fuel cell by coupled genetic algorithm and three-dimensional CFD modeling.* International Journal of Hydrogen Energy, 2020.
34. Wang Z., Wang Y., and Zhuang M., *Improvement of the aerodynamic performance of vertical axis wind turbines with leading-edge serrations and helical blades using CFD and Taguchi method.* Energy conversion and management, 2018. **177**: p. 107-121.
35. Khanjanpour M.H. and Javadi A.A., *Optimization of the hydrodynamic performance of a vertical Axis tidal (VAT) turbine using CFD-Taguchi approach.* Energy Conversion and Management, 2020. **222**: p. 113235.
36. Koutsou C., Kritikos E., Karabelas A. and Kostoglou M., *Analysis of temperature effects on the specific energy consumption in reverse osmosis desalination processes.* Desalination, 2020. **476**: p. 114213.
37. *Tidemap/Tidetech-Maps/https://maps.tidetech.org. Retrieval date: 23/08/2020.*
38. Connor D., Gilliland P., Golding N., Robinson P., Todd D., and Verling E., *UKSeaMap: the mapping of seabed and water column features of UK seas. Joint Nature Conservation Committee, Peterborough.* 2006.
39. Burn S., Hoang M., Zarzo D., Olewniak F., Campos E., Bolto B., and Barron O., *Desalination techniques—A review of the opportunities for desalination in agriculture.* Desalination, 2015. **364**: p. 2-16.
40. Al-Karaghouli A. and Kazmerski L. L., *Energy consumption and water production cost of conventional and renewable-energy-powered desalination processes.* Renewable and Sustainable Energy Reviews, 2013. **24**: p. 343-356.
41. Delgado-Torres A. M., García-Rodríguez L., and del Moral M. J., *Preliminary assessment of innovative seawater reverse osmosis (SWRO) desalination powered by a hybrid solar photovoltaic (PV)-Tidal range energy system.* Desalination, 2020. **477**: p. 114247.

42. Ling C., Lou X., Li J. and Zhang Y., *Experimental investigation of a novel tidal supercharger driven by tidal energy for reverse osmosis seawater desalination*. in *Advances in Renewable Energies Offshore: Proceedings of the 3rd International Conference on Renewable Energies Offshore (RENEW 2018), October 8-10, 2018, Lisbon, Portugal*. 2018. CRC Press.
43. Alkaisi A., Mossad R., and Sharifian-Barforoush A., *A review of the water desalination systems integrated with renewable energy.* Energy Procedia, 2017. **110**: p. 268-274.
44. Shekari Namin A., Rostamzadeh H., and Nourani P., *Thermodynamic and thermoeconomic analysis of three cascade power plants coupled with RO desalination unit, driven by a salinity-gradient solar pond.* Thermal Science and Engineering Progress, 2020. **18**: p. 100562.
45. Ruiz-García A., Melián-Martel N., and Mena V., *Fouling characterization of RO membranes after 11years of operation in a brackish water desalination plant.* Desalination, 2018. **430**: p. 180-185.
46. Alsarayreh A. A., Al-Obaidi M. A., Al-Hroub A. M., Patel R., and Mujtaba I. M., *Performance evaluation of reverse osmosis brackish water desalination plant with different recycled ratios of retentate.* Computers & Chemical Engineering, 2020. **135**: p. 106729.
47. Atallah M. O., Farahat M., Lotfy M. E., and Senjyu T., *Operation of conventional and unconventional energy sources to drive a reverse osmosis desalination plant in Sinai Peninsula, Egypt.* Renewable Energy, 2020. **145**: p. 141-152.
48. Wilf M. and Awerbuch L., *The guidebook to membrane desalination technology: reverse osmosis, nanofiltration and hybrid systems: process, design, applications and economics*. 2007: Balaban Desalination Publications.
49. Qi S., Wang R., Chaitra G. K. M., Torres J., Hu X., and Fane A. G., *Aquaporin-based biomimetic reverse osmosis membranes: Stability and long term performance.* Journal of Membrane Science, 2016. **508**: p. 94-103.
50. Cohen-Tanugi D., McGovern R. K., Dave S. H., Lienhard J. H., and Grossman J. C., *Quantifying the potential of ultra-permeable membranes for water desalination.* Energy & Environmental Science, 2014. **7**(3): p. 1134-1141.
51. Gude G., *Emerging technologies for sustainable desalination handbook*. 2018: Butterworth-Heinemann.
52. Busch M. and Mickols W., *Reducing energy consumption in seawater desalination.* Desalination, 2004. **165**: p. 299-312.
53. Setiawan A. A., Zhao Y., and Nayar C. V., *Design, economic analysis and environmental considerations of mini-grid hybrid power system with reverse osmosis desalination plant for remote areas.* Renewable energy, 2009. **34**(2): p. 374-383.
54. Mohamed E. S., Papadakis G., Mathioulakis E., and Belessiotis V., *The effect of hydraulic energy recovery in a small sea water reverse osmosis desalination system; experimental and economical evaluation.* Desalination, 2005. **184**(1-3): p. 241-246.
55. Chu K. H., Lim J., Kim S. J., Jeong T. U., and Hwang M. H., *Determination of optimal design factors and operating conditions in a large-scale seawater reverse osmosis desalination plant.* Journal of Cleaner Production, 2020. **244**: p. 118918.
56. Alsarayreh A. A., Al-Obaidi M. A., Al-Hroub A. M., Patel R., and Mujtaba I. M., *Evaluation and minimisation of energy consumption in a medium-scale reverse osmosis brackish water desalination plant.* Journal of Cleaner Production, 2020. **248**: p. 119220.

57. Kim J., Park K., Yang D. R., and Hong, S., *A comprehensive review of energy consumption of seawater reverse osmosis desalination plants.* Applied Energy, 2019. **254**: p. 113652.
58. Park K., Kim J., Yang D. R., and Hong S., *Towards a low-energy seawater reverse osmosis desalination plant: A review and theoretical analysis for future directions.* Journal of Membrane Science, 2020. **595**: p. 117607.
59. Karabelas A. J., C. P. Koutsou, M. Kostoglou, and D. C. Sioutopoulos, *Analysis of specific energy consumption in reverse osmosis desalination processes.* Desalination, 2018. **431**: p. 15-21.
60. Fritzmann C., J. Löwenberg, T.Wintgens, and T. Melin, *State-of-the-art of reverse osmosis desalination.* Desalination, 2007. **216**(1-3): p. 1-76.
61. Khanjanpour M. H. and Javadi A. A., *Experimental and CFD Analysis of Impact of Surface Roughness on Hydrodynamic Performance of a Darrieus Hydro (DH) Turbine.* Energies, 2020. **13**(4): p. 928.
62. Badshah M., Badshah S., and Jan S., *Comparison of computational fluid dynamics and fluid structure interaction models for the performance prediction of tidal current turbines.* Journal of Ocean Engineering and Science, 2020. **5**(2): p. 164-172.
63. Meng H., Ma Z., Dou B., Zeng P., and Lei L., *Investigation on the performance of a novel forward-folding rotor used in a downwind horizontal-axis turbine.* Energy, 2020. **190**: p. 116384.
64. Li Y., *On the definition of the power coefficient of tidal current turbines and efficiency of tidal current turbine farms.* Renewable Energy, 2014. **68**: p. 868-875.
65. Bahaj A. S., Batten W. M. J., and McCann G., *Experimental verifications of numerical predictions for the hydrodynamic performance of horizontal axis marine current turbines.* Renewable Energy, 2007. **32**(15): p. 2479-2490.
66. De Lellis M., R. Reginatto, Saraiva R., and Trofino A., *The Betz limit applied to airborne wind energy.* Renewable Energy, 2018. **127**: p. 32-40.
67. Mehmood N., Liang Z., and Khan and J., *CFD study of NACA 0018 for diffuser design of tidal current turbines.* Research Journal of Applied Science, Engineering and Technology, 2012. **4**(21): p. 4552-4560.
68. Zhu F., Ding L., Huang B., Bao M., and Liu J. T., *Blade design and optimization of a horizontal axis tidal turbine.* Ocean Engineering, 2020. **195**: p. 106652.
69. Finnegan W., Fagan E., Flanagan T., Doyle A., and Goggins J., *Operational fatigue loading on tidal turbine blades using computational fluid dynamics.* Renewable Energy, 2020. **152**: p. 430-440.
70. Kulkarni S. S., *Design study of a horizontal axis tidal turbine blade*. 2016, Birmingham City University.
71. Ghasemian M. and Nejat A., *Aerodynamic noise prediction of a Horizontal Axis Wind Turbine using Improved Delayed Detached Eddy Simulation and acoustic analogy.* Energy Conversion and Management, 2015. **99**: p. 210-220.
72. Chen W. H., C. Chen Y., Huang C. Y., and Hwang C. J., *Power output analysis and optimization of two straight-bladed vertical-axis wind turbines.* Applied energy, 2017. **185**: p. 223-232.
73. Bao, Z., Yang F., Wu Z., Nyamsi S. N., and Z. Zhang, *Optimal design of metal hydride reactors based on CFD–Taguchi combined method.* Energy Conversion and Management, 2013. **65**: p. 322-330.

74. Pinar A.M., Uluer O., and Kırmaci V., *Optimization of counter flow Ranque–Hilsch vortex tube performance using Taguchi method.* International journal of refrigeration, 2009. **32**(6): p. 1487-1494.
75. Mandal N., Doloi, B., Mondal B., and Das R., *Optimization of flank wear using Zirconia Toughened Alumina (ZTA) cutting tool: Taguchi method and Regression analysis.* Measurement, 2011. **44**(10): p. 2149-2155.
76. Soorya Prakash K., Gopal P. M., and Karthik S., *Multi-objective optimization using Taguchi based grey relational analysis in turning of Rock dust reinforced Aluminum MMC.* Measurement, 2020. **157**: p. 107664.
77. Phadke, M.S., *Quality engineering using robust design*. 1995: Prentice Hall PTR.
78. Maeda T., Kamada Y., Murata J., Shimizu K., Ogasawara T., Nakai A., and Kasuya T., *Effect of solidity on aerodynamic forces around straight-bladed vertical axis wind turbine by wind tunnel experiments (depending on number of blades).* Renewable energy, 2016. **96**: p. 928-939.
79. Dai Y. and Lam W., *Numerical study of straight-bladed Darrieus-type tidal turbine.* Proceedings of the Institution of Civil Engineers-Energy, 2009. **162**(2): p. 67-76.
80. Kumar P. M., K. Sivalingam, T. C. Lim, S. Ramakrishna, and Wei H., *Strategies for Enhancing the Low Wind Speed Performance of H-Darrieus Wind Turbine—Part 1.* Clean Technologies, 2019. **2**(1): p. 32-51.
81. Brusca S., Lanzafame R., and Messina M., *Design of a vertical-axis wind turbine: how the aspect ratio affects the turbine's performance.* International Journal of Energy and Environmental Engineering, 2014. **5**(4): p. 333-340.
82. Rezaeiha A., Montazeri H., and Blocken B., *Towards optimal aerodynamic design of vertical axis wind turbines: Impact of solidity and number of blades.* Energy, 2018. **165**: p. 1129-1148.
83. Park S. and Rhee S. H., *Influence of blade deformation and yawed inflow on performance of a horizontal axis tidal stream turbine.* Renewable Energy, 2016. **92**: p. 321-332.
84. Zhang H., Guo P., and Sun L., Transient analysis of a multi-unit pumped storage system during load rejection process. Renewable Energy, 2020. 152: p. 34-43.
85. Zhang H., Chen D., Guo P., Luo X., A novel surface-cluster approach towards transient modeling of hydro-turbine governing systems in the start-up process. Energy Conversion and Management, 2018. 165: p. 861-868.
86. Tekade R. K. and Chougule M.B., Formu*lation development and evaluation of hybrid nanocarrier for cancer therapy: Taguchi orthogonal array based design.* BioMed research international, 2013. **2013**.
87. Sohrabi M. R., Khavaran A., Shariati S., and Shariati S., *Removal of Carmoisine edible dye by Fenton and photo Fenton processes using Taguchi orthogonal array design.* Arabian Journal of Chemistry, 2017. **10**: p. S3523-S3531.
88. Banerjee S., Poria S., Sutradhar G., and Sahoo P., *Design of Experiments Analysis of Friction Behavior of Mg-WC Nano-composites using Taguchi Methodology.* Materials Today: Proceedings, 2019. **18**: p. 4026-4033.
89. Ogunbiyi O., Jamiru T., Sadiku R., Adesina O., Olajide J., and Beneke L., *Optimization of spark plasma sintering parameters of inconel 738LC alloy using response surface methodology (RSM).* International Journal of Lightweight Materials and Manufacture, 2020. **3**(2): p. 177-188.

90. Kechagias J. D., Aslani K. E., Fountas N. A., Vaxevanidis N. M., and Manolakos D. E., *A comparative investigation of Taguchi and full factorial design for machinability prediction in turning of a titanium alloy.* Measurement, 2020. **151**: p. 107213.
91. Ranganath M. and Vipin R., *Optimization of Process Parameters in Turning Operation of Aluminium (6061) with Cemented Carbide Inserts Using Taguchi Method and Anova.* International Journal, 2013. **1**(1): p. 13-21.
92. Ott R. L. and Longnecker M. T., *An introduction to statistical methods and data analysis*. 2015: Nelson Education.